Blood Vessel Segmentation from Retinal Images

Anil Maharjan

Master's thesis

School of Computing

Computer Science

June 2016

UNIVERSITY OF EASTERN FINLAND, Faculty of Science and Forestry, Joensuu
School of Computing
Computer Science

Anil Maharjan: Blood Vessel Segmentation from Retinal Images
Master's Thesis, 88 p., 4 appendixes (18 p.)
Supervisor of the Master's Thesis: PhD Pauli Fält
June 2016

Preface

This thesis was done at the School of Computing, University of Eastern Finland during the spring 2016. I would like to express my gratitude to all the people who have helped me in completing this thesis.

First of all, I would like to thank my supervisor PhD Pauli Fält for providing guidelines and suggestions. His valuable comments and help related to subject matters are the key to successfully complete this work. I would also like to thank Professor Markku Hauta-Kasari from University of Eastern Finland and Virpi Alhainen from Natural Resources Institute Finland (Luke) for their motivation and suggestions to accomplish my thesis.

Finally, I would like to express my gratitude to my parents and friends for their constant love and support.

Forssa, June 2016
Anil Maharjan

Abstract

Automatic retinal blood vessel segmentation algorithms are important procedures in the computer aided diagnosis in the field of ophthalmology. They help to produce useful information for the diagnosis and monitoring of eye diseases such as diabetic retinopathy, hypertension and glaucoma.

In this work, different state-of-art methods for retinal blood vessel segmentation were implemented and analyzed. Firstly, a supervised method based on gray level and moment invariant features with neural network was explored. The other algorithms taken into consideration were an unsupervised method based on gray-level co-occurrence matrix with local entropy and a matched filtering method based on first order derivative of Gaussian. During the work, two publicly available image databases DRIVE and STARE were utilized for evaluating the performance of the algorithms which includes sensitivity, specificity, accuracy, positive predictive value and negative predictive value. The accuracies of the algorithms based on supervised and unsupervised methods were 0.935 and 0.950 compared to corresponding values from literature, which are 0.948 and 0.975, respectively. The matched filtering based method produced same accuracy as in the literature, i.e., 0.941.

Although the accuracies of all implemented blood vessel segmentation methods were close to the corresponding values given in the literature the sensitivities were lower for all the algorithms which lead to smaller number of correctly classified vessels from retinal images. Based on the results achieved, the algorithms have potential to be accepted for practical use, after modest improvements are done in order to get better segmentation of retinal blood vessels as well as the background.

Keywords: Retinal vessel segmentation, retinal image, performance measure, supervised method, unsupervised method, matched filtering.

List of abbreviations

Acc	Accuracy
CPU	Central processing unit
DRIVE	Digital Retinal Images for Vessel Extraction (retinal image database)
FDOG	First-order derivative of Gaussian
FOV	Field of view
FPR	False positive rate
GB	Gigabyte
GHz	Gigahertz
GLCM	Gray-level co-occurrence matrix
GMM	Gaussian mixture model
GPU	Graphical processing unit
JPEG	Joint photographic experts group image format
JRE	Joint relative entropy
kNN	K-nearest neighbors algorithm
MF	Matched filter
NN	Neural network
Npv	Negative predictive value
OR	Logical OR operation
PC	Personal computer
PCA	Principal component analysis
PCNN	Pulse coupled neural network
PPM	Portable pixel map image format
Ppv	Positive predictive value
RACAL	Radius based clustering algorithm
RAM	Random access memory
RGB	Red, green and blue color space
Se	Sensitivity
SIMD	Single instruction multiple data
Sp	Specificity
STARE	STructured Analysis of the REtina (retinal image database)
SVM	Support vector machine
TPR	True positive rate
UI	User interface
VLSI	Very large-scale integration

Contents

Appendices

1 Introduction

Retina is the tissue lining the interior surface of the eye which contains the light-sensitive cells (photoreceptors). Photoreceptors convert light into neural signals that are carried to the brain through the optic nerves. In order to record the condition of the retina, an image of the retina (fundus image) can be obtained. A fundus camera system (retinal microscope) is usually used for capturing retinal images. Retinal image contains essential diagnostic information which assists in determining whether the retina is healthy or unhealthy.

Retinal images have been widely used for diagnosing vascular and non-vascular pathology in medical society [1]. Retinal images provide information on the changes in retinal vascular structure, which are common in diseases such as diabetes, occlusion, glaucoma, hypertension, cardiovascular disease and stroke [2, 3]. These diseases usually change reflectivity, tortuosity, and patterns of blood vessels [4]. For example, hypertension changes the branching angle or tortuosity of vessels [5] and diabetic retinopathy can lead to neovascularization i.e., development of new blood vessels. If left untreated, these medical conditions can cause sight degradation or even blindness [6]. The early exposure of these changes is important for taking preventive measure and hence, the major vision loss can be prevented [7].

Automatic segmentation of retinal blood vessels from retinal images would be a powerful tool for medical diagnostics. For this purpose, the segmentation method used should be as accurate and reliable as possible. The main aim of segmentation is to differentiate an object of interest and the background from an image.

1.1 Background

Several methods for the segmentation of retinal image have been reported in literature. Based on machine learning methods, retinal blood vessel segmentation can be divided into two groups: supervised methods [1, 8-11] and unsupervised methods [12-15]. Supervised methods are based on the prior labeling information which clas-

sifies whether a pixel belongs to a vessel or non-vessel class. Whereas, unsupervised methods do not use prior labeling information and have ability to learn and organize information on its own to find the patterns or clusters that resembles the blood vessels.

Filtering or kernel-based methods [16-20] use a Gaussian shaped curve to model the cross-section of a vessel and rotate the matched filters to detect blood vessels with different orientations. Different shaped Gaussian filters such as simple Gaussian model [16-19] and derivative of Gaussian function [20] have been used for blood vessel detection. Another method based on mathematical morphology [21, 22], takes advantage of known vessel features and boundaries and represents them in mathematical sets. Then, using morphological operators, the vessels are extracted from the background.

Vessel tracking based methods as proposed by [21, 23] try to acquire the vasculature structure by following vessel center lines. Usually a set of start points are established and then the vessels' traces are generated based on local information, attempting to find the path that best matches the vessel profile model. In model-based methods, clearly stated vessel models are applied to detect the blood vessels. These methods utilize active contour or snake models [24], vessel profile model [25, 26] and geometric model based on level set method (LSM) [27] for blood vessel segmentation.

1.2 Motivation

Manual segmentation of the retinal blood vessels is arduous and time-consuming, and making a detailed segmentation can be challenging if the complexity of the vascular network is too high [4]. Thus, automated segmentation is valuable, as it decreases the time and effort required, and in the best case scenario, an automated algorithm can provide as good or better segmentation results as an expert by manual labeling [6]. For practical applications, it would be better to have algorithms that do not critically depend on configuring many parameters so that also non-experts may utilize this technology with ease [28]. Automated blood vessel segmentation has

faced challenges related to low contrast in images, wide range of vessel widths and variety of different structures in retinal images such as retinal image boundaries, optic disc and retinal lesions caused by diseases [29]. Even though, different methods are available for retinal segmentation, there is still space for improvement.

Mostly, the algorithms for retinal blood vessel segmentation concentrate on automatic detection related to diabetic retinopathy, which is found to be the major cause of blindness in recent days. Vision loss related to diabetic retinopathy can be prevented if the disease is discovered in an early stage [30]. Hence, many authors have proposed several different blood vessel segmentation approaches based on different techniques. The complexities and segmentation performances vary among the algorithms. In this thesis, different blood vessel segmentation algorithms are studied, implemented and their performance is compared with the results provided in the literature.

1.3 Research questions

Blood vessel segmentation is a challenging task. Although numerous algorithms have been proposed for retinal blood vessel segmentation, a "gold-standard" method is still unavailable. Some methods possess comparatively higher accuracies and vessels detection capabilities, while others have only moderate ones. The three state-of-art methods [8, 12, 20] from three different categories (i.e. supervised, unsupervised, and match filtering methods) were selected for detailed study and implementation. The selection is based on their higher accuracy rates compared to other algorithms within the same categories. Hence, the selection of these methods arises first research question

1. How accurate are the selected blood vessel segmentation methods in extracting blood vessels from fundus images?

Different literature reviews related to the retinal blood vessel segmentation give in-depth information about the usability and expected results of different methods [8,12, 16, 20, 21]. This motivates the another research question

2. Are automated blood vessel extraction methods trustworthy compared to manual segmentation done by experts?

The main goal of this thesis is to answer the research questions.

1.4 Structure of the thesis

Chapter 2 presents the physiological background related to the structure of the human eye and the functionality of its components. It also includes the materials used for evaluating the algorithms that were implemented during the study of different retinal vessel segmentation methods. It is followed by brief introduction of different types of vessel segmentation methods proposed by different authors. Furthermore, the chapter explains the three different categories for vessel segmentation methods: supervised, unsupervised and matched filtering along with detailed explanation of one method from each category.

Chapter 3 contains the detailed processes that were followed during the implementation of three different vessel segmentation methods. It includes the algorithms' workflow followed by the calculation of their performance measures.

Chapter 4 describes the results obtained from the implemented algorithms and also compares the corresponding performance measures with the original authors' results.

Chapter 5 presents the thesis' conclusions based on the experimental results and also the achievements from the study.

2 Materials and methods

2.1 Structure of the human eye

Human eye is the light-sensitive organ that enables one to see the surrounding environment. It can be compared to a camera in a sense that the image is formed on the retina of eye while in a traditional camera the image is formed on a film. The cornea and the crystalline lens of the human eye are equivalent to the lens of a camera and the iris of the eye works like the diaphragm of a camera, which controls the amount of light reaching the retina by adjusting the size of pupil [31]. The light passing through cornea, pupil and the lens reaches the retina at the back of the eye, which contains the light sensitive photoreceptors. The image formed on the retina is transformed into electrical impulses and carried to the brain through the optic nerves, where the signals are processed and the sensation of vision is generated [32]. The general diagram of human eye is shown in Figure 1.

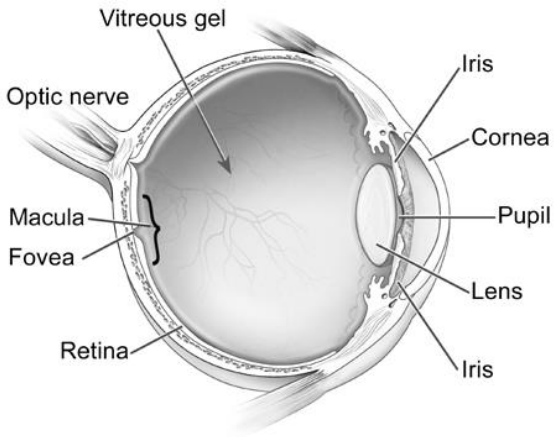

Figure 1. The structure of the human eye (image is taken from [33]).

The small, yellowish central area of the retina which is around 5.5 mm in diameter is known as macula [34]. The macula and its center area (fovea) provide sharp central vision. A healthy macula can provide at least a normal (20/20) vision [35]. Fovea is densely populated with ‘cone’ photoreceptors which are responsible for the trichromatic human color vision. Fovea contains no ‘rod’ photoreceptors which provide

information on brightness. The L-, M- and S-cone cells are sensitive to long, middle, and short wavelength ranges in the visible part of the electromagnetic spectrum (i.e., 380-780 nm), respectively, whereas rod cells provide no color information [34].

Optic disc is the visible part of the optic nerve where the optic nerve fibers and blood vessels enter the eye. It does not contain any rod or cone photoreceptors, so it cannot respond to light. Thus, it is also called a blind spot. The retinal arteries and veins emerge from the optic disc. Retinal arteries are typically narrower than veins. Macula fovea, optic disc, veins and arteries are illustrated in Figure 2.

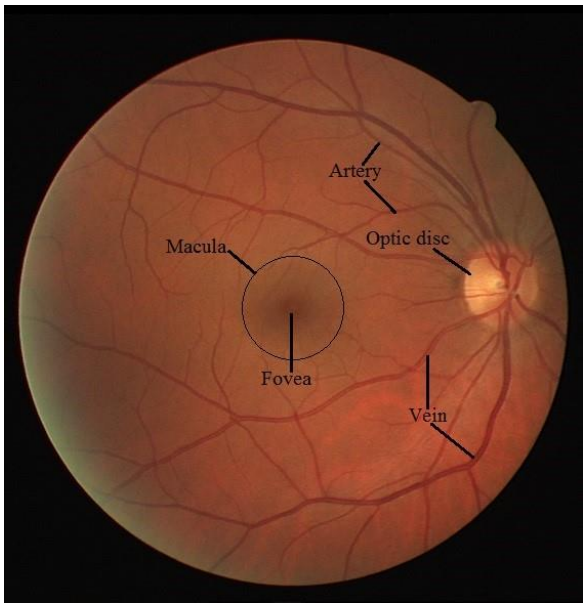

Figure 2. Fundus image (image is taken from [36]).

2.2 Materials

The vessel segmentation methodologies were evaluated by using two publicly available databases containing the retinal images, DRIVE [36] and STARE [37]. The DRIVE database contains 40 retinal color images among which seven contain signs of diabetic retinopathy. The images have been captured using Canon CR5 non-mydriatic 3-CCD camera with a 45° field of view (FOV). Each image has 768×584 pixels with 8 bits per color channel in JPEG format. The database is divided into two groups: *training set* and *test set*, each containing 20 images. The training set con-

tains color fundus images, the FOV masks for the images, and a set of manually segmented monochrome (black and white) ground truth images. The test set contains color fundus images, the FOV masks for the images, and two set of manually segmented monochrome ground truth images by two different specialists. The ground truth images of the first observer were used for measuring the performance of algorithms.

The STARE database for blood vessel segmentation contains 20 color retinal images among which ten contain pathology. The images have been taken using TopCon TRV-50 camera with 35° FOV. Each image has 700×605 pixels with 8 bits per color channel in PPM format. This database does not have separate training and test sets as in DRIVE. It also contains two sets of manually segmented monochrome ground truth images by two different specialists. The manually segmented images by the first human observer were used as the ground truth for evaluating the performance of the algorithms.

2.3 Blood vessel segmentation classification

There are several techniques for blood vessel segmentation and diagnosis of diseases related to retina. Different authors have categorized those methods in different way. In [21], the authors divided the retinal vessel segmentation into seven main categories; (1) pattern recognition techniques, (2) matched filtering, (3) mathematical morphology, (4) multiscale approaches, (5) vessel tracking, (6) model based approaches, and (7) parallel/hardware based approaches. Pattern recognition deals with classification of retinal blood vessels and non-vessels together with background, based on key features. This approach has two methods; supervised and unsupervised. If a priori information is used to determine a pixel as a vessel or not, then that method is supervised, otherwise it is unsupervised method. Matched filtering uses convolution of two dimensional kernels, which is designed to model a feature at some position and orientation, with the retinal image and detect vessels by maximizing the responses of kernels used [2, 4]. Mathematical morphology deals with the mathematical theory of

representing shapes like features, boundaries, etc. using sets. Mainly two morphological operators; erosion and dilution, are used for applying structuring element to the images. Two algorithms; Top hat and watershed transformations are popularly used in medical image segmentation [21]. The combination of multiscale enhancement, fuzzy filter and watershed transformation is used to extract vessels from retinal image [22]. As the vessel moves away from the optic disc, its diameter decreases. The idea behind multiscale approach is to use the vessel's width to determine blood vessels having varying width at different scales [21]. Many of the multiscale algorithms are based on the vessel enhancement filter which is described by Frangi et al. [38]. And in [39], the vessel detection is obtained from fast discrete curvelet transform and multi-structure mathematical morphology. Vessel tracking method segments a vessel between two points by identifying vessel center line rather than entire vessels at once [21, 23]. In this method, the tracing of the vessel, which seems like a line, is done by using local information and by following vessel edges. Model based approach uses fully and clearly expressed vessel models to extract blood vessels. The models like snake or active contour model [25], multi-concavity modelling method [26], Hessian-based technique [40] are some of the methods used in this approach. Parallel hardware based approach is mainly for fast and real time performance, and implementation is done in hardware chips. The implementation of this approach for real time image processing is done in VLSI chip by representing cellular neural network [41]. In [42], morphological operations and convolutions are implemented together with arithmetic and logical operations to extract blood vessels in single instruction multiple data (SIMD) parallel processor array.

According to [4], vessel segmentation methods are grouped into three categories; (1) pixel processing-based, (2) tracking-based, and (3) model-based approaches. Pixel processing-based approach measures features for every pixel in an image and classifies each pixel in either vessel or non-vessel class. It includes two processes: initial enhancement of the image by applying convolution and secondly adaptive thresholding and morphological operations followed by classification of vessel pixels. Pattern recognition based, matched filtering, and multiscale based approaches mentioned in

[21] have resemblance with pixel processing-based method. While tracking-based and model-based approaches are similar to that as mentioned in [21].

Another authors [2] have categorized vessel segmentation into three different methods; (1) kernel-based, (2) tracking based and (3) classifier-based. The kernel-based method consists matched filtering, and mathematical morphology, while tracking based is same as mentioned in [21]. Pattern recognition based approach as referred in [21] is similar to the classifier-based method. This shows that even different authors have different way of classifying the blood vessel segmentation, the main idea remains same. Some authors want to elaborate the classification by defining detail characteristics per approach while others combined two or more characteristics to form a single approach and briefing the number of approaches.

Pattern recognition-based approaches like supervised and unsupervised methods, and matched filtering-based methods are explained in detail in the following sections.

2.4 Supervised methods

Pattern recognition is the process of classifying input data into objects or classes by the recognition and representation of patterns it contains and their relationships [43, 44]. It includes measurement of the object to identify attributes, extraction of features for the defining attributes, and comparison with known patterns to determine the class-memberships of objects; based on which classification is done. Pattern recognition is used in countless applications, such as computer aided design (CAD), in medical science, speech recognition, optical character recognition (OCR), finger print and face detection, and retinal blood vessel segmentation [43, 45]. It is generally categorized according to the classification procedures. Classification is the procedure for arranging pixels and assigning them to particular categories. The features used for characterization of pixels can be texture, size, gray band value, etc. A set of extracted features is called a feature vector. The general procedure used in classification is as follows:

i. *Classification classes definition:* Depending upon the objective and characteristics of the image data, the classes into which the pixels are to be assigned, are determined.
ii. *Feature selection:* The features like texture, gray band value, etc. are selected for classification.
iii. *Characterize the classes in terms of the selected features:* Usually two sets of data with known class-memberships are defined; one for training and other for testing the classifier.
iv. *Defining the parameters (if any) required for the classifier:* The parameters or appropriate decision rules, required by the particular classification algorithm are determined using the training data.
v. *Perform classification:* Using the trained classifier (e.g., a maximum likelihood classifier, or a minimum distance classifier), and the class decision rules, the testing data are classified to the classes.
vi. *Result evaluation:* The accuracy and reliability of the classifier are evaluated based on the test data classification results.

Based on the classification method, pattern recognition can be either supervised or unsupervised [43]. Supervised classification is the procedure in which user interaction is required: user defines the decision rules for each class/pixels or provides training data for each class/pixels to guide the classification. It uses supervised learning algorithm for creating a classifier, based on training data from different object classes. The input data are provided to the classifier, which assigns the appropriate label for each input. Whereas unsupervised method attempts to identify the patterns or clusters from the input dataset without predefined classification rules [46]. It learns and organizes information on its own to find the proper solution [47].

In blood vessel segmentation, the supervised method is based on pixel classification, which utilizes the a priori labeling information to determine whether a pixel belongs to a vessel or non-vessel. All pixels in image are classified into vessel or non-vessel class by the classifier. In image classification, the training data is considered to represent the classes of interest. The quality of training data can significantly influence

the performance of an algorithm and thus, the classification accuracy [48], which suggests to choose proper training data. Feature extraction and the selection of parameters for the classier are also critical because they assist in determining the accuracy and overall result of the classification algorithm. The classifiers are trained by supervised learning with manually processed and segmented ground truth image [8, 21]. The ground truth image is precise and usually marked by an expert or ophthalmologist. Different kinds of classifiers, such as neural networks, Bayesian classifier, support vector machine etc., have been used for improving classification [49, 50]. Similarly, various feature vectors have been used in supervised methods for blood vessel segmentation, like Gabor feature, line operator, gray-level and moment invariants [1, 8, 9]. The preceding section describes a supervised method of blood vessel segmentation using gray-level and moment invariant based features with neural network as classifier.

2.4.1 Gray level and moment invariant based features with neural network

The term '*gray-level*' refers to the intensity of a particular pixel in the image. In segmentation of image using supervised method, the sequence of gray levels of pixel's neighbors can be used as a feature vector [51]. A feature vector is a vector that contains information describing an object's important characteristics. Image moments and moment invariants could help in object recognition and its analysis [52]. Moment invariants use the idea of describing the objects by a set of measurable quantities called invariants that are unresponsive to particular deformations and that provide enough information to distinguish among objects belonging to different classes. The image processing technique that uses gray level and moment invariants based features with neural network can be explained in four different stages (see Figure 3): Preprocessing of retinal image for gray level homogenization and blood vessel enhancement, feature extraction, classification of pixel to label it as vessel or non-vessel, and post-processing for removing falsely detected isolated vessel pixels [8].

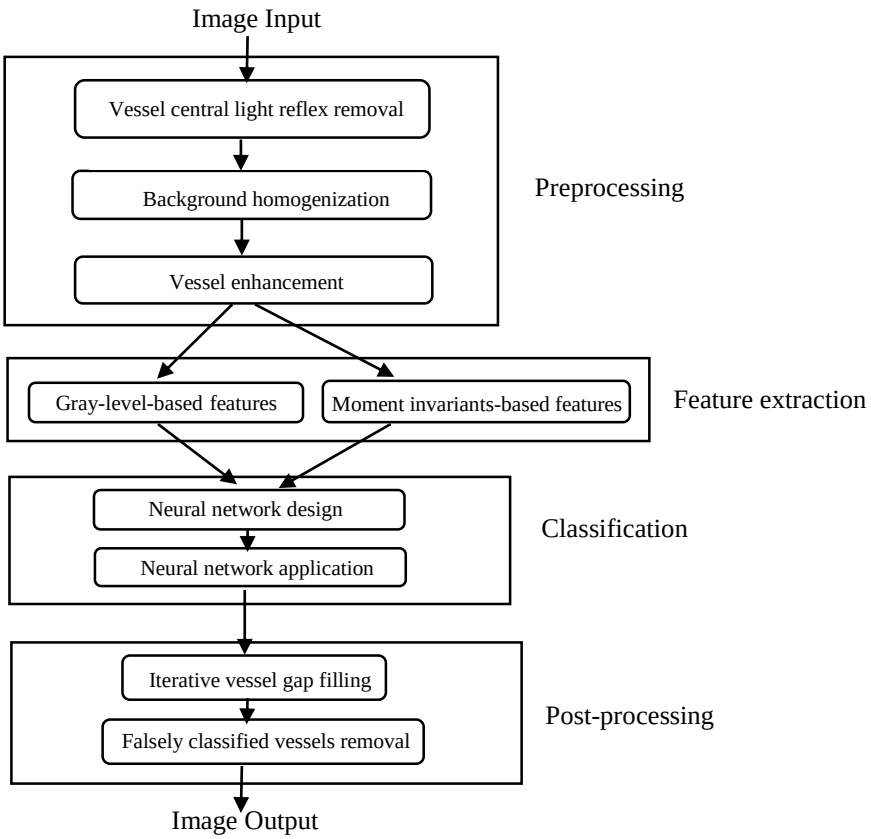

Figure 3. Steps for blood vessel segmentation using Gray level and moment invariants features with neural network.

2.4.1.1 Preprocessing

The retinal image usually has imperfections like poor contrast and noise, which need to be reduced or eliminated before extracting pixels' features for classification. So preprocessing is necessary step to be followed, which includes different sub-steps. In general, retinal blood vessels have lower reflectance and appear darker than other structures in a retinal image. Typically, bright areas known as light reflex can be seen in the center of blood vessels. For blood vessel segmentation, it is useful to remove these bright reflections from the retinal image. Often, the green channel of an RGB (red/green/blue) image is extracted because it provides better vessel-background contrast than red or blue channels, and can thus be used for identifying blood vessels from retinal images [53]. By applying morphological opening to the green channel of image, the bright central lines can be removed from the blood vessels as shown in Figure 4(b).

Due to the non-uniform illumination, the fundus image often consists of some background pixels, which have intensity values comparable to the brighter vessel pixels (center light reflex) [8]. Those pixels can degrade the performance of segmentation algorithm, as the gray-level values are used to form feature vector that is used to represent a pixel in the classification stage. Those background lightening variations should be removed, and a shade-corrected image is generated; for example, as follows: Initially, the occasional salt and pepper noise is removed by using *3 x 3* mean filter, and the resultant image is convoluted with a Gaussian kernel of dimension *m x m = 9 x 9, mean = 0,* and *standard deviation = 1.8*, which further reduces the noise and is denoted by I_g. Secondly, I_g is passed through *69 x 69* mean filter, which blurs the retinal image and yields the background image, I_b. The difference between I_g and I_b is calculated for every pixel, and the result is used for generating shade-corrected image:

$$D(x, y) = I_g(x, y) - I_b(x, y) \quad (1)$$

Lastly, the shade-corrected image (I_{sc}) is generated by transforming linear intensity values into the possible gray levels (8-bit image: 0-255) values (see Figure 4(c)).

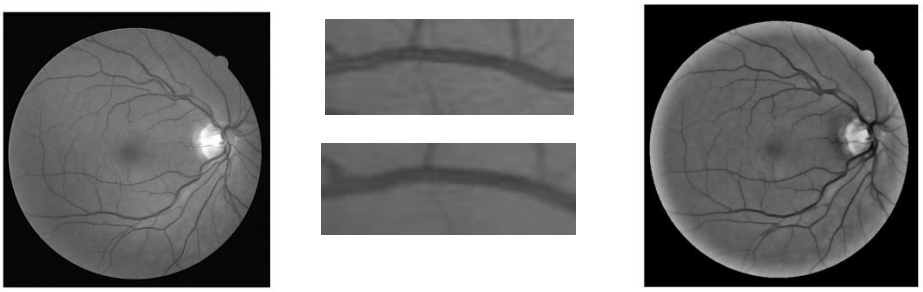

(a) (b) (c)

Figure 4. Example of Preprocessing stage: (a) Green channel of original retinal image (DRIVE database image 2, [36]) (b) Upper part is from green channel image that contains central light reflex, and in lower part, central light reflex is removed, (c) Shade-corrected image.

Moreover, during image acquisition process, different illumination conditions are possible which results in significant variations in intensities of images. This is minimized by forming homogenized image I_h, using gray-level transformation function:

$$g_{\text{Output}} = \begin{cases} 0, & if\ g < 0 \\ 255, & if\ g > 255 \\ g, & otherwise \end{cases} \quad (2)$$

where,

$$g = g_{\text{Input}} + 128 - g_{\text{Input\_max}} \quad (3)$$

Here, g_{Input} and g_{Output} are the gray level variables of input (I_{sc}) and output (I_h) respectively and $g_{\text{Input\_max}}$ is the gray level value of input (I_{sc}), which has highest number of pixels. The homogenized image is shown in Figure 5(b).

The final step during preprocessing is to obtain vessel enhanced image I_{ve}, which is generated by applying white top hat transformation to the complemented homogenized image (I_h). Top hat transformation is used to correct the uneven background illumination [54]. Vessel enhanced image I_{ve} is

$$I_{ve} = I_h^c - \gamma(I_h^c) \quad (4)$$

where I_h^c is the complemented homogenized image and γ is morphological opening operator. This vessel enhanced image helps in extraction of moment invariant based features and is shown as in Figure 5(c).

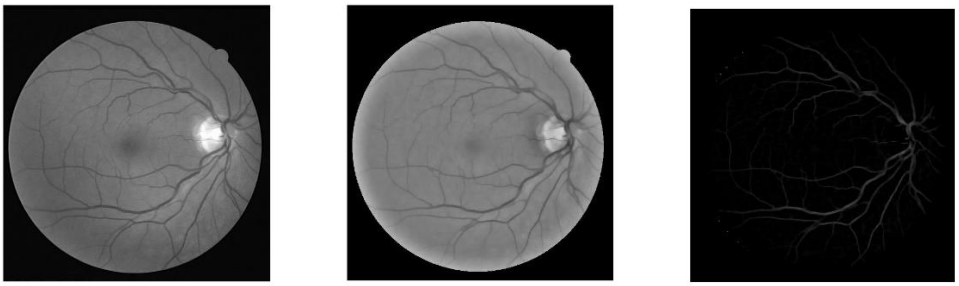

(a) (b) (c)

Figure 5. Example of Preprocessing stage: (a) Green channel of original retinal image (DRIVE database image 2, [36]) (b) Homogenized image, (c) Vessel-enhanced image.

2.4.1.2 Feature extraction

Image features are distinctive attributes or aspects of image, which is important in image processing. The features which are extracted from the image are useful in classifying and recognition of image [55]. And the features extracted during this

phase helps in classifying pixels whether it belongs to vessel or not. Two different kind of features; *gray level based features* and *moment invariant based features* are extracted [8].

A. Gray level based features

Blood vessels are usually darker than background in the green channel image. So the gray levels of pixels on vessels are smaller than gray levels of other pixels in a local area. This statistical gray level information of vessels can be used to obtain the features from retinal image [56]. Gray level features in retinal image are based on the difference between the gray level in vessel pixel and a statistical value of its surrounding local pixels. The homogenized image, I_h is used to generate a set of gray level based features for each image pixel (x, y) by operating only on a small image area (window) centered at (x, y). The feature vectors are calculated as:

$$f_1(x,y) = I_h(x,y) - \min_{(s,t)\epsilon S^9_{x,y}} \{I_h(s,t)\} \tag{5}$$

$$f_2(x,y) = \max_{(s,t)\epsilon S^9_{x,y}} \{I_h(s,t)\} - I_h(x,y) \tag{6}$$

$$f_3(x,y) = I_h(x,y) - \operatorname{mean}_{(s,t)\epsilon S^9_{x,y}} \{I_h(s,t)\} \tag{7}$$

$$f_4(x,y) = \operatorname{std}_{(s,t)\epsilon S^9_{x,y}} \{I_h(s,t)\} \tag{8}$$

$$f_5(x,y) = I_h(x,y) \tag{9}$$

where $S^w_{x,y}$ is set of co-ordinates having window size of $w \times w$ and window center point at *(x, y).*

B. Moment invariant based features

Invariant moments have had a great impact on image recognition or classification and have been widely used as features for recognition in many areas of image processing. They are popular because of having property which does not change with rotation, scale and translation [57, 58]. Hence invariant moments are computed for each separate block and the result is compared with the target image blocks for finding the similarity.

The two-dimensional moment of order $(p + q)$ for image $f(x, y)$ can be obtained as:

$$m_{pq} = \sum_x \sum_y x^p y^q f(x, y) \text{ where p, q = 0, 1, 2 …} \quad (10)$$

Consider a small block of image defined by region $S_{x,y}^{17}$ from vessel enhanced image I_{ve} and a pixel as (x, y), having window size of 17×17. Then its moment is calculated as

$$m_{pq} = \sum_i \sum_j i^p j^q I_{ve}^{S_{x,y}^{17}}(i, j) \quad (11)$$

where $I_{ve}^{S_{x,y}^{17}}$ is the gray level at point (i, j). And the central moment is defined as

$$\mu_{pq} = \sum_i \sum_j \left(i - \bar{i}\right)^p (j - \bar{j})^q I_{ve}^{S_{x,y}^{17}}(i, j) \quad (12)$$

where, $\bar{i} = \frac{m_{10}}{m_{00}}$ and $\bar{j} = \frac{m_{01}}{m_{00}}$ are the centroid of the image. Similarly, the normalized central moment is defined as

$$\eta_{pq} = \frac{\mu_{pq}}{(\mu_{00})^{(\frac{p+q}{2}+1)}} \quad \text{where } p + q = 2, 3, \ldots \quad (13)$$

The concept of moment invariant is introduced by Hu, and based on normalized central moments, a set of seven different moment invariants are defined, among which first two are enough to obtain optimal performance reducing the computation complexity [8, 59]. The two moments taken into consideration are:

$$\emptyset_1 = \eta_{20} + \eta_{02} \quad (14)$$

$$\emptyset_2 = (\eta_{20} + \eta_{02})^2 + 4\eta_{11}^2 \quad (15)$$

According to [8], the moment invariants obtained from $I_{ve}^{S_{x,y}^{17}}$ are not useful to define the central pixel of the sub-image as a vessel or non-vessel. So the new sub-image I_{hu} is generated to surpass that problem. I_{hu} is produced by multiplying the original vessel enhanced sub-image $I_{ve}^{S_{x,y}^{17}}$ with a Gaussian filter of window size=17×17, mean=0 and variance=1.7^2. Hence, the new sub-image is described as:

$$I_{hu}(i, j) = I_{ve}^{S_{x,y}^{17}}(i, j) \times G_{0,1.7^2}^{17}(i, j) \quad (16)$$

Using I_{hu}, first and second moment invariants are generated. So these moment invariant features for pixel located at (x, y) can be obtained as:

$$f_6(x, y) = |log(\emptyset_1)| \tag{17}$$

$$f_7(x, y) = |log(\emptyset_2)| \tag{18}$$

2.4.1.3 Classification

The seven features for each pixel obtained from feature extraction process is characterized by a vector in a seven-dimensional feature space as:

$$F(x, y) = [f_1(x, y), f_2(x, y), \dots, f_7(x, y)] \tag{19}$$

These features are used in classification process in which every candidate pixel is classified as either a vessel pixel (C_1) or non-vessel pixel (C_2). According to [8], the use of a linear classifier results in relatively poor ability to separate classes in vessel segmentation, which creates a need for a non-linear classifier. There are few non-linear classifiers like Bayesian classifier, support vector machine, kNN classifier and neural network. For implementation of blood vessel segmentation, a neural network (NN) is used as a non-linear classifier.

Neural network is defined as a computing system consisting of a number of simple, interconnected processing elements, which respond to and process information from external inputs [60]. Neural networks are typically organized in layers consisting of a number of interconnected 'nodes', which contain an 'activation function' [61]. Input data are presented to the network via the 'input layer', which transfers input data to one or more 'hidden layers' where the actual processing is done via a system of weighted 'connections'. The 'output layer' gets result from hidden layer and transfer that output for corresponding agent.

The classification process for blood vessel segmentation is divided into two phases: Neural network design, and neural network application. A multilayer feedforward network with adequate neurons in a single hidden layer can approximate any function, provided the activation function of the neurons satisfies some general con-

straints [62]. But according to [8], a multilayer feedforward network with an input layer, three hidden layers and an output layer provides better results. An input layer consists of seven neurons, five for gray-level features and two for moment invariant features. While each hidden layer consists of 15 neurons and an output layer contains only one neuron as an output (see Figure 6) [21]. The output is passed through a linear sigmoid activation function, which generates value between 0 and 1.

Before training the neural network, the features obtained from feature extraction process are normalized, as their values and ranges differ, by using

$$\overline{f}_i = \frac{f_i - \mu_i}{\sigma_i} \tag{20}$$

where μ_i and σ_i are mean and standard deviation of ith features f_i. The training image's features, as mentioned in Eq. (20), are used as training data and the ground truth image data which contains the classification results for that image data are subjected to neural network. For NN training, the back propagation training is used which makes NN to adjust its connection weights depending upon the error feedback, so it learns and reduces error [8, 63].

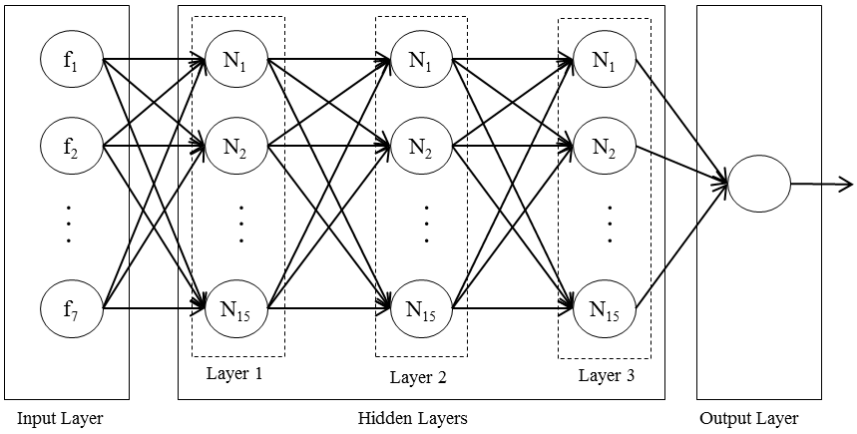

Figure 6. Neural network showing an input layer with seven nodes, three hidden layers with 15 nodes on each layer and one node in output layer.

After the trained NN is generated, test data is passed through the trained NN to obtain blood vessels from retinal images. Since the sigmoid function is used at the output end, the output results have value ranging between 0 and 1. And since the classification rule for each pixel has only two class values, either vessels (C_1) or non-

vessels (C_2), thresholding is required. Considering a threshold T_h and applying it on each candidate pixel produces a classification output image I_{co} so that classes C_1 and C_2 are associated to gray levels 255 and 0, respectively, as follows:

$$I_{co}(x,y) = \begin{cases} 255\ (\equiv C_1), & if\ p\big(C_1 \big| F(x,y)\big) \geq T_h \\ 0\ (\equiv C_2), & Otherwise \end{cases} \tag{21}$$

where $p\big(C_1 \big| F(x,y)\big)$ denotes the probability of a candidate pixel (x,y) to belong to a vessel class C1 as explained by the feature vector $F(x,y)$ [8]. The thresholded image is shown in Figure 5(b).

2.4.1.4 Post processing

The post processing stage is another import operation to obtain better and accurate segmentation. Usually during this stage, the noise produced by the classification stage is removed. It is divided into two steps: iterative filling of pixel gaps in detected blood vessels, and falsely detected isolated vessel pixel removal.

The vessels might have gaps which are vessel pixels but have been classified as non-vessels. By applying iterative filling procedure these gaps can be filled. This is done by considering that each candidate pixel with at least six neighbors classified as vessel points must also belong to a vessel [8, 29]. The next step is to remove falsely classified vessel pixels, for which first get the number of pixels in each connected region, and reclassify to those pixels by labeling as a non-vessel each pixel that has less than 25 vessel-pixels in a region connected to it [8]. By increasing or decreasing the limiting pixel count, the accuracy and sensitivity of the blood vessel segmentation can be adjusted. The post processed image is presented in Figure 7(c).

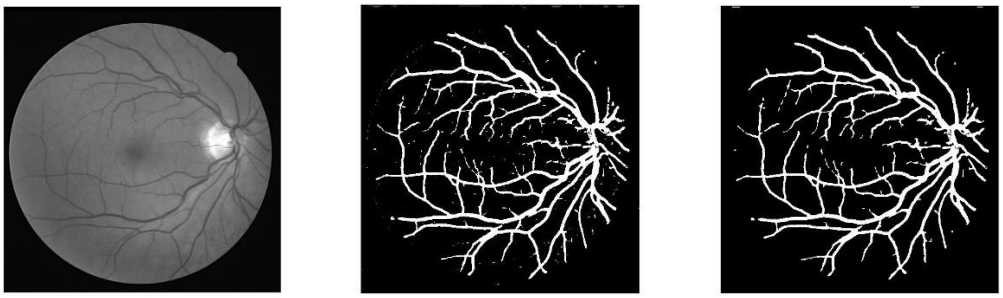

(a) (b) (c)

Figure 7. (a) Green channel of the original retinal image (DRIVE database image 2, [36]) (b) Thresholded image, (c) Post-processed image

2.4.2 Other supervised methods for retinal image segmentation

Many authors had introduced different kinds of supervised methods for retinal blood vessel segmentation. The use of supervised classification using a Gaussian mixture model classifier (Bayesian classifier) to classify each pixel as either a vessel or a non-vessel, and two-dimensional Gabor wavelet as a feature vector has been illustrated by Soares et al. [64]. This approach does not work well for non-uniformly illuminated retinal images as it generates false detection at the border of the optic disc, and with certain types of pathologies with strong contrast.

Ricci and Perfetti [9] introduced a support vector machine (SVM) for pixel classification and line operators as feature vectors. In comparison to other supervised methods, this method requires less features, with simpler computation while feature extraction and fewer features are needed for training. As the method uses local differential computation of line strength, it overcomes the problem related to non-uniform illumination and contrast as faced by Soares et. al [62]. The combination of radial projection and SVM was used by You et al. [65], in which vessel centerline was located using radial projections and line strength measure was used to generate a feature vector.

Niemeijer [66] used a feature vector that contained the green channel of RGB image and the responses of a Gaussian matched filter and its first and second order derivatives. In order to classify a pixel as a vessel or a non-vessel, k-nearest neighbor (k-

NN) classifier was used. Staal [10] also used a k-NN classifier for classification in his ridge based vessel segmentation algorithm. The features used are based on the ridge of the image and total of 27 features are used to form a feature vector.

A supervised method using an AdaBoost classifier was introduced by Lupascu et at. [46]. They used a relatively large number of features, about 41, to form a feature vector. The features include various vessel related descriptions like, local (pixel's intensity and Hessian-based measures), structural (vessel's geometric structures), and spatial (gray-level profile approximated by Gaussian curve).

Shadgar and Osareh use a multiscale Gabor filter for vessel identification and principal component analysis (PCA) for feature extraction [47]. The classification algorithms like Gaussian mixture model (GMM) and SVM are used for classifying a pixel as vessel or non-vessel. Besides the algorithms mentioned above, there are also other supervised blood vessel segmentation methods, which are not included here.

2.5 Unsupervised methods

Unsupervised learning is another method used in pattern recognition. In supervised methods, class-labels of the training data are known beforehand. In unsupervised methods, neither the classes nor the assignments of the training data to the classes are known. Instead, unsupervised methods try to identify patterns or clusters in the training data [46]. Unsupervised methods have an ability to learn and organize information but do not give error signals that could be used to evaluate the performances of the given potential solutions [47]. Sometimes this can be advantageous, since it enables the algorithm to look back for patterns that have not been previously considered [67].

The goal of unsupervised learning is to model the underlying structure or distribution in the data in order to learn more about the data. Algorithms are left on their own to discover and present interesting structures in the data. Sometimes unsupervised learning provides superior, and broadly usable, alternative to established methods, especially for problems that haven't been solved clearly by supervised method [68].

Unsupervised methods have been used in various applications such as Natural Language Processing (NLP), data mining, fraud analysis, remote sensing image classification, object recognition, and also retinal image segmentation.

In retinal blood vessel segmentation, the unsupervised classification tries to find fundamental patterns of blood vessels, which is used to determine whether a pixel is vessel or non-vessel. In this method, the training data or gold standard image does not help directly to design the algorithm [21]. Various authors have proposed different retinal image segmentation methods. The method by Villalobos-Castaldi et al. [12] using local entropy information with gray-level co-occurrence matrix (GLCM) has yielded relatively better results than others. The reported results for accuracy, sensitivity and specificity are 0.9759, 0.9648 and 0.9759 respectively, for DRIVE retinal images.

2.5.1 Local entropy and gray-level co-occurrence matrix

In general, a single generally acknowledged vessel segmentation algorithm does not exist due to the unique properties of each acquisition technique. Every segmentation method has some challenges in detecting vessels precisely when applied alone. In this method, a combination of two methods, matched filtering and co-occurrence matrix with entropy thresholding, are applied to detect retinal blood vessels. Hence, the retinal image segmentation, as described by Villalobos-Castaldi et al. [12], based on local entropy and gray-level co-occurrence matrix is divided into three different stages: blood vessel enhancement using matched filter, gray-level co-occurrence matrix computation, and segmentation of extracted blood vessel using joint relative entropy thresholding. The workflow of this method is illustrated in Figure 8.

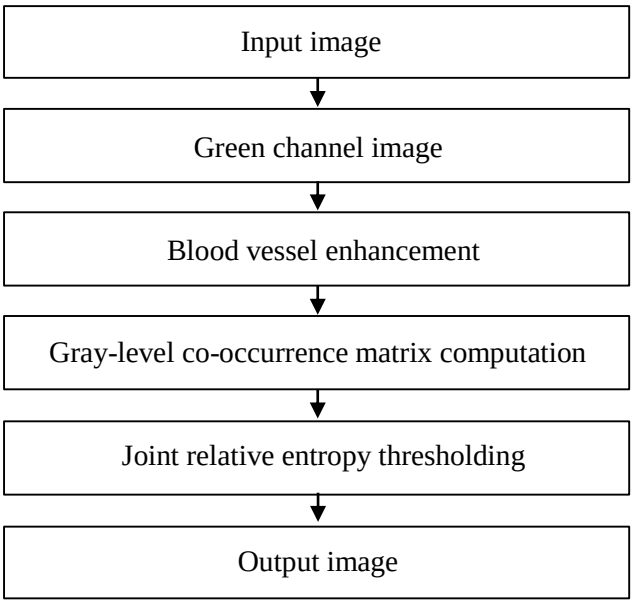

Figure 8. Flowchart of unsupervised method of segmentation using joint relative entropy and co-occurrence matrix.

2.5.1.1 Blood vessel enhancement using matched filter

Since blood vessels appear darker compared to the background, the vessels should be enhanced before proceeding. Hence, the green channel of an RGB retinal image is extracted as it provides better vessel-background contrast than red or blue channels [53]. The green channel image is used for further processing with matched filter. Usually blood vessels do not have absolute step edges and gray-level intensity profile varies in every blood vessel [69]. The intensity profile of a cross section of a blood vessel can be modeled by a Gaussian shaped curve [17], which is shown in Figure 13(a). Hence, a matched filter can be used for the detection of piecewise linear segments of blood vessels in retinal images [70]. The two dimensional matched filter kernel is convolved with the green channel retinal image to enhance the blood vessels. According to Chaudhuri et al. [17], the two dimensional Gaussian matched filter can be expressed as:

$$f(x,y) = -exp\left(-\frac{x^2}{2\sigma^2}\right) \ \forall\ |y| \leq \frac{L}{2} \tag{22}$$

where σ is the scale of the filter or the spread of the intensity profile and L is the length of the vessel segment having the same orientation. The kernel is rotated along 12 possible directions by 15 degree steps to form 12 different templates because the vessels can be oriented in any direction [12, 13]. The kernel with $\sigma = 2$ matches well with the medium sized vessels in retinal images used [12]. A retinal image is convolved individually by each of the 12 kernels with different orientations and, from the set of these 12 output images, the maximum value for each pixel (x,y) is selected to form the matched filter response image (Figure 12(b)). This enhancement method extracts the blood vessels and also lowers the possibility of false detection of blood vessels [12, 17].

2.5.1.2 Gray-level co-occurrence matrix computation

Texture is an important characteristic that has been used for classifying and recognizing the objects. It can be represented by spatial distribution of gray levels in its surrounding area [71]. Haralick et al. [72] introduced a two dimensional texture analysis matrix known as gray-level co-occurrence matrix (GLCM) in 1973 for acquiring the spatial dependence of gray level values, which became one of the widely used feature extraction methods in image processing. The values of the co-occurrence matrix show relative frequencies P_{ij} in which two neighboring pixels separated by distance d appear on the image, where one of them has gray level i and other has j [14]. GLCM computation not only depends on the displacement but also on the orientation between the neighbor pixels [73]. Normally the angle between two pixels is considered to be 0º, 45º, 90º or 135º. The four directions of a pixel for calculating co-occurrence matrix's values is shown in Figure 9.

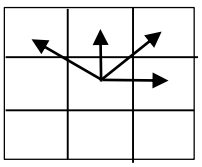

Figure 9. The four directions of a pixel for calculating co-occurrence matrix's values.

Consider an image of size $M \times N$ with L gray levels expressed by $G = \{0, 1, 2, \dots, L-1\}$ and the gray level of pixel at location (m, n) be $f(m, n)$. The co-occurrence matrix of an image is a $L \times L$ square matrix, which can be denoted as $W = [t_{ij}]_{L \times L}$, where t_{ij} is the number of transitions from gray level value i to gray level value j [69]. The value of t_{ij} can be calculated as

$$t_{ij} = \sum_{m=1}^{M} \sum_{n=1}^{N} \delta_{mn} \tag{23}$$

$$\text{where, } \delta_{mn} = \begin{cases} 1, \ if \begin{cases} f(m,n) = i \ and \ f(m+1,n) = j \\ and/or \\ f(m,n) = i \ and \ f(m,n+1) = j \end{cases} \\ 0, \ other \ wise \end{cases}$$

An example related to co-occurrence matrix is shown in Figure 10, where an image intensity represented by a 4×4 matrix is used as input. Four different co-occurrence matrixes are generated based on four orientations 0º, 45º, 90º and 135º among the adjacent pixels.

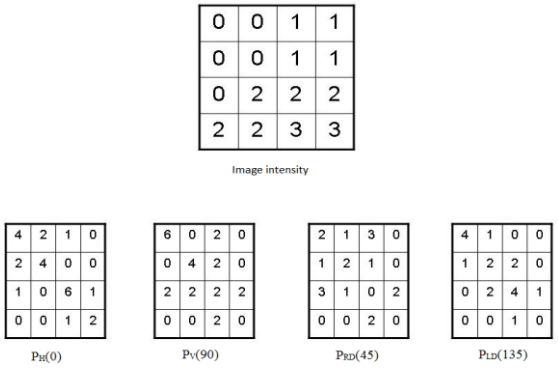

Figure 10. Co-occurrence matrix generation for gray level $L = 4$ and four different offsets: PH (0◦), PV (90◦), PRD (45◦), and PLD (135◦).

The transition probability P_{ij} from gray level *i* to *j* can be written as

$$P_{ij} = \frac{t_{ij}}{\sum_{k=0}^{L-1} \sum_{l=0}^{L-1} t_{kl}} \tag{24}$$

Consider *t* as the threshold used on the image, which divides the co-occurrence matrix into four quadrants, namely *A, B, C*, and *D* as shown in Figure 11 and Eq. (25). According to [69], the gray level value of pixel above the threshold is labeled as

foreground while value below or equal to the threshold is labeled as background. The quadrant *A* corresponds to transition within background (*BB*) and *C* within foreground (*FF*). Similarly, the quadrants *B* and *D* correspond to the transition between background and foreground, which are represented by *BF* and *FD* respectively.

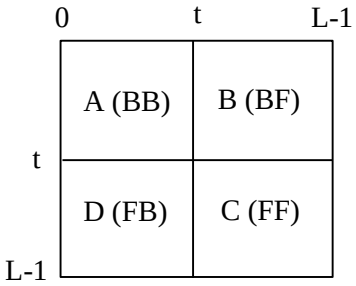

Figure 11. Four quadrants of a co-occurrence matrix.

The probabilities of each quadrant is defined as

$$P_A^t = \sum_{i=0}^{t}\sum_{j=0}^{t} P_{ij} \qquad P_B^t = \sum_{i=0}^{t}\sum_{j=t+1}^{L-1} P_{ij}$$
$$P_C^t = \sum_{i=t+1}^{L-1}\sum_{j=t+1}^{L-1} P_{ij} \qquad P_D^t = \sum_{i=t+1}^{L-1}\sum_{j=0}^{t} P_{ij} \tag{25}$$

These probabilities are used in the next Section.

2.5.1.3 Joint relative entropy thresholding

Image entropy is defined as a measure of uncertainty that characterizes the texture of the input image. Relative entropy between two probability distributions is a measure of the information distance between them [69]. The two probability distributions are closer to each other if the relative entropy is smaller and vice versa. Consider two sources having *L* gray levels and probability distributions *p* and *h*. Then the relative entropy between these probability distributions is given by

$$J(p;h) = \sum_{j=0}^{L-1} p_j log \frac{p_j}{h_j} \tag{26}$$

In Eq. (26), the entropy is calculated as *h* relative to *p*. Here, *p* is considered as the original image and *h* as the processed image that tries to match with *p*. The co-

occurrence matrix can be used to expand the first order relative entropy into second order joint relative entropy (Eq. 27). Let t be the threshold value and h_{ij}^t the transition probability of the thresholded image. Then the cell probabilities of the thresholded image in all four quadrants are defined as

$$h_{ij|A}^t = q_A^t = \frac{P_A^t}{(t+1)(t+1)} \qquad h_{ij|B}^t = q_B^t = \frac{P_B^t}{(t+1)(L-t-1)}$$

$$h_{ij|C}^t = q_C^t = \frac{P_C^t}{(L-t-1)(L-t-1)} \qquad h_{ij|D}^t = q_D^t = \frac{P_D^t}{(L-t-1)(t+1)} \tag{27}$$

Using Eq. (25) and Eq. (27), Eq. (26) can be expressed as

$$\begin{aligned} J(\{p_{ij}\};\{h_{ij}^t\}) &= \sum_{i=0}^{L-1}\sum_{j=0}^{L-1} p_{ij}\, log\, \frac{p_{ij}}{h_{ij}^t} \\ &= -H(\{p_{ij}\}) - \sum_{ij} p_{ij} log\, h_{ij}^t \\ &= -H(\{p_{ij}\}) - (P_A^t log q_A^t + P_B^t log q_B^t + P_C^t log q_C^t + P_D^t log q_D^t) \end{aligned} \tag{28}$$

where $H(\{p_{ij}\})$ is the entropy of $\{p_{ij}\}_{i=0,j=0}^{L-1,L-1}$, which is independent of threshold t and is expressed as $H(\{p_{ij}\}) = -\sum_{i=0}^{L-1}\sum_{j=0}^{L-1} p_{ij}\, log p_{ij}$. According to [69], the proper threshold value for segmenting foreground (vessels) from background can be obtained by taking quadrants *B* and *D* into consideration. Hence, only using $P_B^t log q_B^t + P_D^t log q_D^t$ from Eq. (28) gives more effective edge detection. Therefore, the joint relative entropy (JRE) threshold can be defined as

$$t_{jre} = \arg[\min_{t\epsilon G} H_{jre}(t)] \tag{29}$$

where,

$$H_{jre}(t) = -(P_B^t log q_B^t + P_D^t log q_D^t) \tag{30}$$

Entropy $H_{jre}(t)$ is obtained by considering all gray pixels within quadrants *B* and *D*, and the optimal value t_{jre} from Eq. (29) is the threshold value used for segmenting the retinal image. An example of a final segmented retinal image is shown in Figure 12(c).

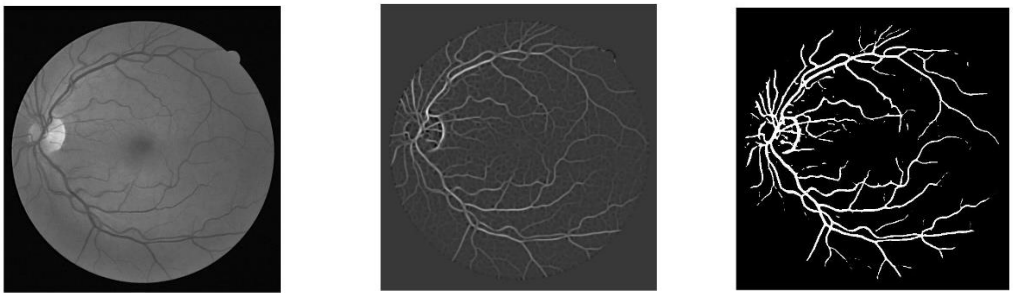

(a) (b) (c)

Figure 12. Original green channel retinal image (DRIVE database image 1 [36]), (b) Blood vessel enhanced with matched filter, and (c) JRE thresholded image.

2.5.2 Other unsupervised methods for retinal image segmentation

Besides the unsupervised methods using a gray-level co-occurrence matrix for retinal blood vessel segmentation, there are other techniques proposed by different authors. Kande et al. [13] proposed an unsupervised vessel segmentation method which applies matched filtering for blood vessel enhancement and spatially weighted fuzzy C-means clustering along with labeling based on connected components for blood vessel extraction.

Simo and Ves [74] used a Bayesian image analysis technique to segment blood vessels from retinal images. The method uses Markov random fields' prior probability model to describe retinal image information and statistical parameter estimation for segmentation. This method is found to be strong against salt and pepper noise.

A vessel detection system based on maximum likelihood model of retinal image is proposed by Ng et al. [75]. Initially it applies second derivative Gaussian filters over a retinal image to produce a filter response. Secondly, it creates a Gaussian model of noise and calculates the covariance of filter output to isotropic noise. The image and noise models are subjected to maximum likelihood estimator to generate model parameters such as width, contrast and direction of blood vessels for every pixel along with likelihoods of the model with additive noise. By using vessel parameters and likelihoods, the vessel's centerline is detected, which is combined with width parameter to locate the vessels.

Salem et al. [76] developed a radius based clustering algorithm (RACAL) that uses a distance based rule to map the distributions of the image pixels. It uses features like local maxima of the gradient magnitude and local maxima of large eigenvalue obtained from a Hessian matrix. The method combines a clustering algorithm with a partial supervision strategy.

2.6 Matched filtering

Retinal blood vessels can be detected using methods based on filter operators. Matched filtering is a pattern matching algorithm based on the structural properties of the object to be identified or recognized [16]. The expected appearance of a desired signal or object can be described by a matched filter [19]. The use of matched filter to detect retinal blood vessels has been carried out by Chaudhuri et al. [17], which makes use of a priori knowledge that cross-section of vessels can be approximated by Gaussian function, which suggested that matching the blood vessels can be done using a Gaussian shaped filter. According to Chaudhuri et al. [17], retinal blood vessels possess three different characteristics:

- The blood vessels have small curvatures and may be approximated by piecewise linear segmentation.
- The width of blood vessel decreases when moving away from the optic disk.
- Due to lower reflectance of vessels in comparison to other retinal structures, they seem to be darker compared to the background.

Using matched filtering, image's features can be detected, which are most similar to a predefined template [17]. In this method, blood vessels are assumed to be piecewise linear segments with cross sectional intensity changes similar to a predefined kernel [18]. As blood vessels can have different spatial orientations, a set of kernels is required to detect the vessels. An adequate number of kernels to detect vessels with different orientations is considered to be 12, which are produced by rotating each kernel by 15 degrees apart from the previous one [16, 17, 77]. The matched filter kernel can be expressed as [20]:

$$K(x,y) = \frac{1}{\sqrt{2\pi}\sigma}\exp\left(-\frac{x^2}{2\sigma^2}\right) - m \quad for\ |x| \le t\sigma\ , |y| \le \frac{L}{2} \tag{31}$$

where,

$$m = \frac{\left(\int_{-t\sigma}^{t\sigma} \frac{1}{\sqrt{2\pi}\sigma}\exp\left(-\frac{x^2}{2\sigma^2}\right)dx\right)}{(2t\sigma)} \tag{32}$$

is the normalizing factor. And L is the length of the vessel segment having same orientation and σ is the scale of filter or spread of intensity profile. Normalizing the mean value of filter to 0 aids in removing smooth background after filtering. About 99% of the area under Gaussian curve lies within range of $[-3\sigma, 3\sigma]$, hence the constant, t is set to value of 3. The parameter L is chosen based on the value of σ. The smaller the value of σ, L needs to be set relatively smaller as well, and vice versa. According to [17], the best parameter values of L and σ which give maximum response are at $L = 9$ and $\sigma = 2$.

Since 12 different kernels, rotated at 15 degree steps, are enough for determining the all possible vessels, every pixel of the image is convolved with these kernels. The result obtained after examining all the pixels produces output image which consists of dark pixels denoting non-vessels whereas bright pixels belong to the vessels [18]. According to Chaudhuri et al. [17], when both the kernel and vessel have same orientation, then the pixel response is maximum.

2.6.1 First-order derivative of Gaussian

Matched filter (MF) has ability to respond to both the vessels' and non-vessels' edges. This problem can be seen in Figures 13(a), (b1) and (b2), which show the response of a MF to a Gaussian function (i.e. cross section of a vessel) and a step edge (i.e. non-vessel). It is hard to separate vessels only by using MF because both vessels and non-vessels will be detected after applying threshold over MF response. Hence, an extra filter is also required along with MF, which in this case is the first-order derivative of Gaussian (FDOG) filter [20].

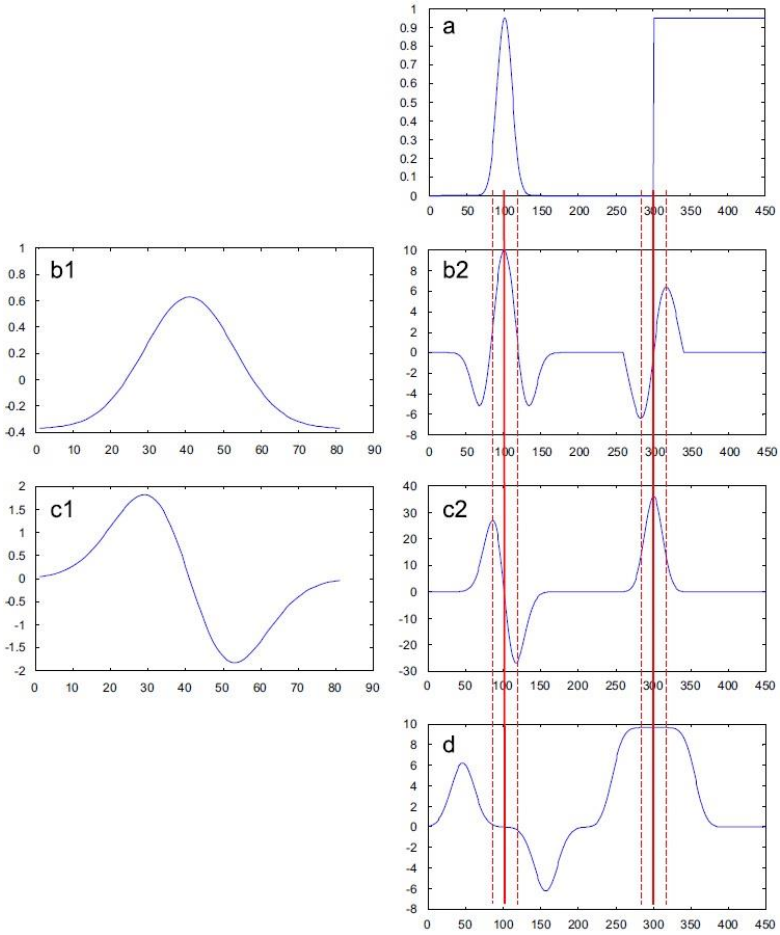

Figure 13. Responses of the matched filter (MF) and the first-order derivative of Gaussian (FDOG) to a Gaussian line cross section and an ideal step edge: (a) a Gaussian line cross-section and an ideal step edge, (b-1) the MF and (b-2) its filter response, (c-1) the FDOG and (c-2) its filter response and (d) the local mean of the response to the FDOG [20].

The Gaussian derivative has a special property. The result obtained from the product of two Gaussians yields a Gaussian as a result, and also their convolution gives a Gaussian function [78]. Furthermore, Gaussian's even order derivatives (including the zeroth order which is Gaussian function itself) are even functions (i.e. symmetric around zero) while the odd order derivatives are odd functions (i.e. antisymmetric around zero) which is illustrated in Figure 14.

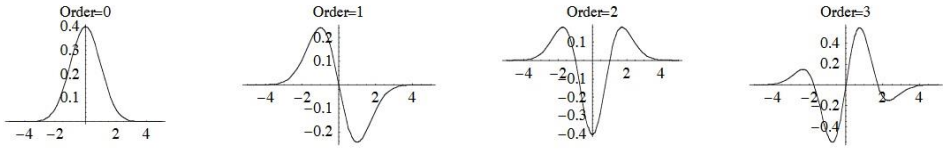

Figure 14. Plots of derivatives of a Gaussian for orders from 0 to 3 [79].

Mathematically, the first order derivative of Gaussian matched filter, which is defined in Eq. (31), can be written as

$$K(x,y) = -\frac{x}{\sqrt{2\pi}\sigma^3}\exp\left(-\frac{x^2}{2\sigma^2}\right) \quad for\ |x| \le t\sigma\ , |y| \le \frac{L}{2} \tag{33}$$

Figure 13 shows that the response of Gaussian function is strong, and positive for the MF and anti-symmetric for FDOG. On the other hand, the non-vessel step edge's response for FDOG is strong and symmetric but anti-symmetric for MF [20]. If a threshold T is applied to MF response, it detects both vessels and non-vessels, and leads to wrong classification. Hence, the thresholding needs to be applied to the MF response image but the threshold value is adjusted based on the image's response to FDOG [20].

Consider h as the MF response and d as FDOG response as illustrated in Figures 13 (b-2) and (c-2). The local mean of d, d_m is the response obtained as the average of neighboring pixels as shown in Figure 13 (d). Since the retinal image is filtered twice, by MF and by FDOG, the two responses H and D are generated respectively. And as the threshold value is adjusted using FDOG, the local mean of D can be calculated by applying a mean filter over D as

$$D_m = D * W \tag{34}$$

where W is a mean filter with a window size of $w \times w$. The local mean image D_m is normalized and denoted as $\overline{D}_m$, which is used to generate the threshold value. The threshold value T can be obtained by

$$T = (1 + \overline{D}_m)T_c \tag{35}$$

where Tc is the reference threshold which is calculated as

$$T_c = c \times \mu_H \tag{36}$$

where c is constant value that is usually between 2 and 3 and μ_H is the mean value of the MF response H [20]. The threshold T obtained in Eq. (35) is applied to H in order to get final segmented image I_H, which can be presented as

$$I_H = \begin{cases} 1 & H(x,y) \geq T(x,y) \\ 0 & H(x,y) < T(x,y) \end{cases} \quad (37)$$

An example of the final segmented image along with original and ground truth images are illustrated in Figure 15.

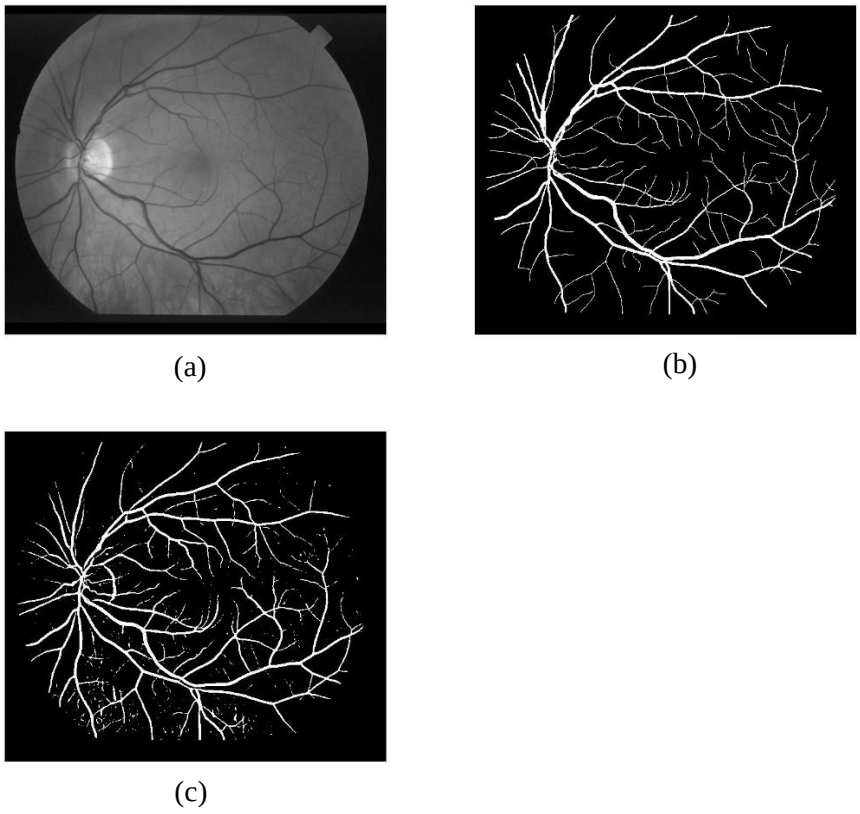

(a) (b)

(c)

Figure 15. (a) Original green channel retinal image (STARE database image 162 [37]), (b) Ground truth image and (c) Blood vessels extracted using MF-FDOG.

2.6.2 Other matched filtering methods for retinal image segmentation

The first two-dimensional linear Gaussian filter used for the segmentation of retinal blood vessels was proposed by Chauduri et al. [17]. The Gaussian filter or kernel is rotated by 15 degree steps to match the different orientations of blood vessels. For every pixel, the largest response value is selected and used as a threshold value to segment the retinal blood vessels. Chauduri's matched filter concept was improved by Al-Rawi et al. [16] using an exhaustive search optimization technique. This meth-

od finds the optimal matched filter size and threshold value which is applied to the input retinal image and obtained segmented image.

Hoover et al. [19] used threshold probing technique on a matched filter response image along with local and region-based features of a retinal image for segmentation. This method analyzes the matched filter response image in pieces. With iterative probing, a threshold is applied to each pixel and each pixel is classified as a vessel or a non-vessel. The method produced approximately 75% true positive rate and also 15 times smaller false positive rate than the basic thresholding of matched filter response.

The combination of a matched filter and an ANT colony algorithm for retinal image segmentation is suggested by Cinsdikici and Aydin [80]. A preprocessed retinal image is passed through a matched filter and ANT algorithm in parallel fashion and the results are combined together. After applying length filtering over the result, the retinal blood vessels are extracted.

Yao and Chen [81] proposed a two-dimensional Gaussian matched filter for blood vessel enhancement. A pulse coupled neural network (PCNN) is applied for segmentation which produces multiple results. Furthermore, among the number of segmentation results, the best results are selected by using a 2-D-Otsu algorithm. After analyzing the local connectivity among the pixels, the final segmented retinal image is obtained. There are also other methods related to retinal blood vessel segmentation based on matched filtering technique, but they are not considered in the scope of this thesis.

3 Implementation

The implementation of all three blood vessels segmentation processes was done in Matlab by creating separate application for each process. The applications were tested using the retinal images from the publicly available databases: DRIVE [36] and STARE [37]. These databases also include the ground truth images for all the available retinal images. While testing the application, the ground truth image of the same retinal image is used as gold standard to compare with the output of the algorithm and produce the performance measure values for evaluating the algorithm's accuracy. The implementations of individual segmentation processes are explained below.

3.1 Supervised method using gray-level and moment invariants with neural network

While implementing this method, the entire process is divided into four distinct steps:

i. Preprocessing
ii. Feature extraction
iii. Classification
iv. Post-processing

Initially, a training set of retinal images is used to generate a trained multilayer feed-forward neural network. During the process, the input image is preprocessed in order to reduce image imperfection like noise, poor contrast and lightning variation [8]. The preprocessing step includes removal of brighter strips by applying morphological opening, followed by generating shade-corrected image to produce background homogenized image. This result is further processed by using Top-Hat transformation to remove bright retinal structures (i.e., reflection artifacts, optic disc). The processed image is then subjected to the module which generates five gray-level and two moment invariants features. The Matlab codes for generating features are divided into multiple function listed in Appendix B. The generated features are used to

create a trained neural network. The process diagram for generating features is shown in Figure 16.

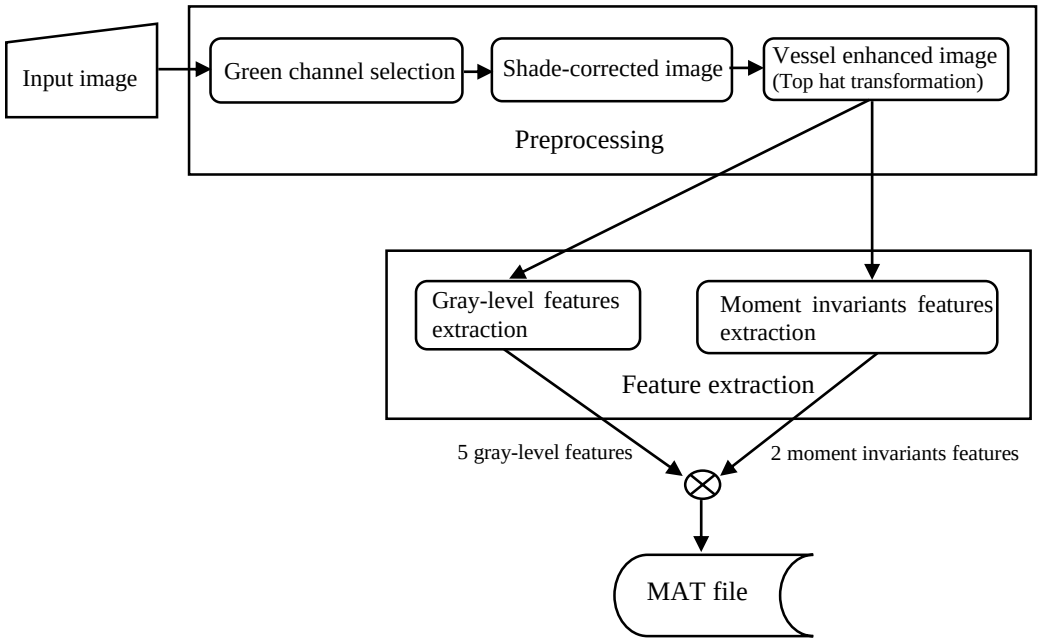

Figure 16. Flow chart of preprocessing and feature extraction mechanism.

While training the neural network, the expert's hand sketched binary vessel segmentation image is used as a ground truth of the given retinal image. For training the classifier, the ground truth images from the training set are used, while during test phase, test set's ground truth images are used. For training NN, the features which are extracted as described above, and target data (i.e. ground truth) are subjected to the feed-forward backpropagation network. Originally, the network was designed with an input layer, three hidden layers, each with 15 neurons and an output layer [8]. But the performance results, when tested with DRIVE and STARE images were found to be relatively poor, with only a small number of the vessel pixels correctly detected. Therefore, in this thesis, a different neural network was used. The new implementation has a network consisting of an input layer, a single hidden layer containing 20 neurons for DRIVE images and 15 for STARE images, and an output layer (see Figure 17). These parameters provided better results than three hidden layers. For training a neural the network, Matlab's built-in function '*feedforwardnet'* with

its default configuration is used. Once the training is done, the trained neural network is generated, which is ready for simulation with test data.

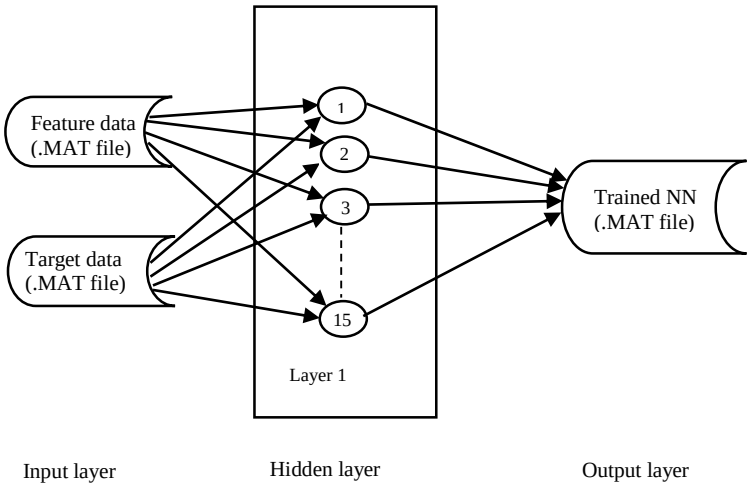

Figure 17. A feed-forward backpropagation neural network with two input layers, three hidden layers, a single output layer.

Secondly, the images from the test set are used for testing the trained neural network (simulation). Before simulation, the test image's features are extracted by following the similar steps as during the neural network generation. Then the features of the test image are subjected to the simulation process with the trained neural network which results in a vessel segmentation output image. In order to produce binary segmentation images for the segmented retinal blood vessel images in the DRIVE dataset, the threshold is set to 53% of the maximum value; whereas for the STARE dataset, threshold is set to 43% of the maximum value (see Figure 18). The resulting image still has both detected vessels and falsely detected isolated vessel pixels. The flowchart showing the thresholding process to generate segmented vessel image is illustrated in Figure 18.

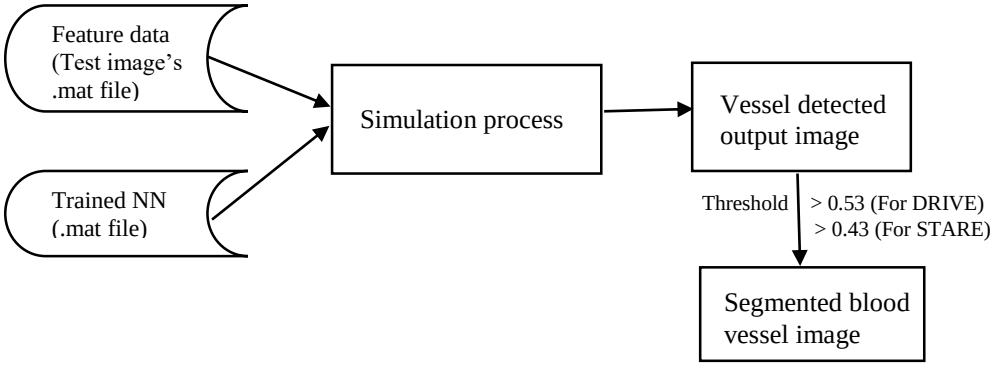

Figure 18. Flowchart of simulating test image with trained neural network.

Finally, the segmented blood vessel output image is passed through a post-processing module to fill the pixel gaps in detected vessels and to remove falsely detected vessels. For iterative filling, the 8-neighborhood around each pixel is taken into account. If the neighbors are vessel pixels, then the pixel is classified as a vessel. After classification, misclassified pixels are removed depending on the size of connected area. If the pixel's connected area consists of less than 10 vessel-pixels, the pixel is marked as a non-vessel. After post-processing steps the final output image is produced, which is used to calculate the performance measures of the algorithm being implemented. The calculated measures are sensitivity, specificity, positive predictive value, negative predictive value, and accuracy using formulas as described in [8] (Tables I and II).

Table I: Performance measure calculation formula

Sensitivity (Se) = $\frac{TP}{TP+FN}$
Specificity (Sp) = $\frac{TN}{TN+FP}$
Positive predictive value (Ppv) = $\frac{TP}{TP+FP}$
Negative predictive value (Npv) = $\frac{TN}{TN+FN}$
Accuracy (Acc) = $\frac{TP+TN}{TP+FN+TN+FP}$

where,

Table II: Vessel classification [8].

	Vessel present	**Vessel absent**
Vessel detected	True Positive (TP)	False Positive (FP)
Vessel not detected	False Negative (FN)	True Negative (TN)

Sensitivity (*Se*) and specificity (*Sp*) are the ratios of correctly classified vessels and non-vessels respectively. While Positive predictive value (*Ppv)* is the ratio of pixels correctly classified as vessel pixel and negative predictive value (*Npv*) is the ratio of pixels correctly classified as background. Accuracy is measured as the ratio of correctly classified pixels to the total number of pixels in field of view (FOV) [8]. The function for calculating performance measures is implemented in Matlab code as listed in Appendix B.

During implementation, the training and test datasets were taken from same database. For example, the training set data from DRIVE database were used to generate a trained NN and test set data were used for testing. Similarly, for STARE database, its own training set and test set data were used for obtaining a trained NN and for testing. Two training set images, one from DRIVE and STARE databases were also combined to form a single training image and used for generating a trained NN. The test result from this approach did not give any significant improvement in the result. While training, the learning rate is also varied to get better results. The value of 5% for learning rate gave better results than higher values, which obviously increased the time required for training a NN. In general, the time requirement for training a NN was around half an hour for 5 % learning rate. The test results, more specifically accuracy and sensitivity, of DRIVE image dataset are comparatively better than for STARE image dataset (see Table III and IV).

3.2 Unsupervised method using local entropy and gray-level co-occurrence matrix

The application development process is divided into four distinct steps: vessel extraction based on matched filter, co-occurrence matrix generation, second-entropy thresholding segmentation and performance measurement.

First the input image's green channel is extracted which is used to extract retinal vessel using matched filter technique. The matched filter response is obtained by using specific values for σ (spread of the intensity profile), *yLength* (length of the neighborhood along y-axis), and Θ (number of orientations) over the given image. The values used for extracting thick blood vessels are σ=1.2, *yLength*=9 and Θ=12. While extracting matched filter response, the vessels are extracted from the number of orientations being used, which is 12 in this case. The response images for the 12 filters are stacked as a three-dimensional data cube with the response images as layers. The maximum response along the third dimension is chosen be the final response of the matched filter, which is considered to be the thick vessels being extracted. Once the response image is obtained, it is multiplied with the mask in element-wise fashion, and then normalized, so the values lie between 0 and 1. The flowchart of the algorithm is shown in Figure 19.

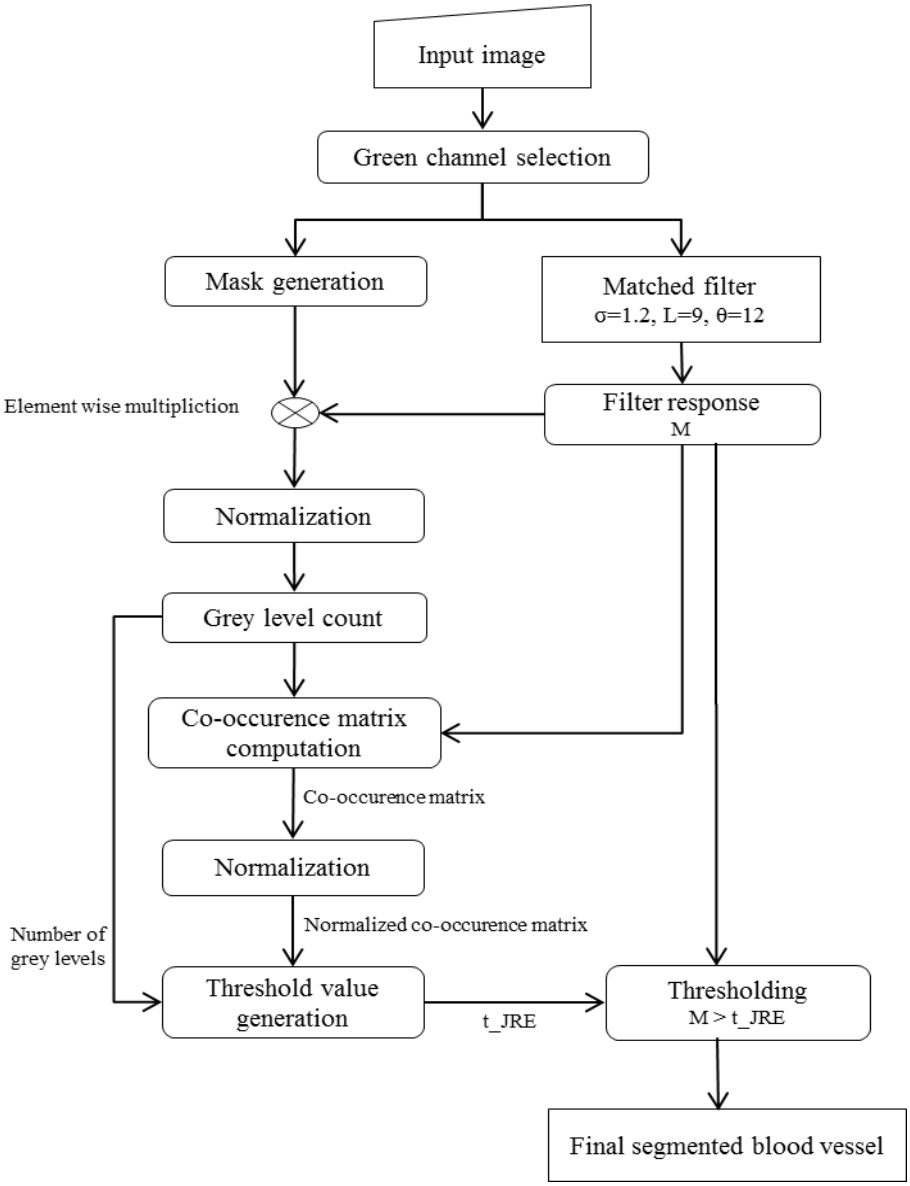

Figure 19. Overall process diagram of the unsupervised method for retinal vessel segmentation using local entropy and co-occurrence matrix.

The second step, co-occurrence matrix generation, needs the count of gray levels from the previously extracted vessel image. During this step, the response image is multiplied by 255 (for an 8-bit image) and rounded to ceiling value in order to get distinct gray level count. Matlab's built-in function '*graycomatrix*' is used for calculating co-occurrence matrix, which is being used in developing this application.

Before generating the second entropy threshold value and applying it over the matched filtered response to get final extracted vessel, the gray co-occurrence matrix,

being calculated in previous step, is normalized first. The co-occurrence matrix is passed to a function along with the total number of gray levels, which are present in matched filtered image. The function defined for calculating threshold value iterates over entire number of gray-levels being passed as argument and calculate probabilities associated with two quadrants: B and D as shown in Figure 11.

The function for calculating the threshold value is implemented in Matlab code as listed in Appendix C. The value obtained from the above function is used for thresholding the matched filter image response giving the final segmented retinal image, which is the basis for performance measure calculation. Using the test retinal images, sensitivity, specificity, positive predictive value, negative predictive value, and accuracy were calculated to realize the algorithm's performance (see Table I and II).

During implementation, the mask for DRIVE images is generated using threshold value 20/255, whereas for STARE images it's 35/255. Different threshold values were tried to see their effect of the algorithm's performance. When the threshold values were smaller or larger than the threshold values specified above, vessel segmentation performance was poorer. Different values for σ and *yLength* were also tested for generating matched filtered response. The σ value of 1.2 yields better performance results than others, whereas *yLength's* value 9 yields decent results. When *yLength's* value is increased, more noise is produced even though specificity is increased. Similarly, when its value is decreased, the segmented image has poorer vessel detection capability as well as poorer performance results.

3.3 Matched filter using first order derivative of Gaussian

The implementation process includes: generation of thick and thin vessels, performing logical OR to obtain blood vessels and performance measurement (see Figure 20). Initially, the green channel of the input retinal image is extracted which is passed to the function that generates the segmented blood vessel images, which contains either thick or thin vessels based on the parameters provided. The function takes seven different parameters as arguments in order to produce the segmented

blood vessels. Those parameters are green channel image, mask image, σ (spread of the intensity profile), *yLength* (length of the neighborhood along y-axis), Θ (number of orientation), constant (*c_value* for calculating reference threshold *Tc*), and threshold (*T*) value for Matlab-function 'regionprops', which measures properties like area, convex hull, centroid, etc., of image regions or connected components.

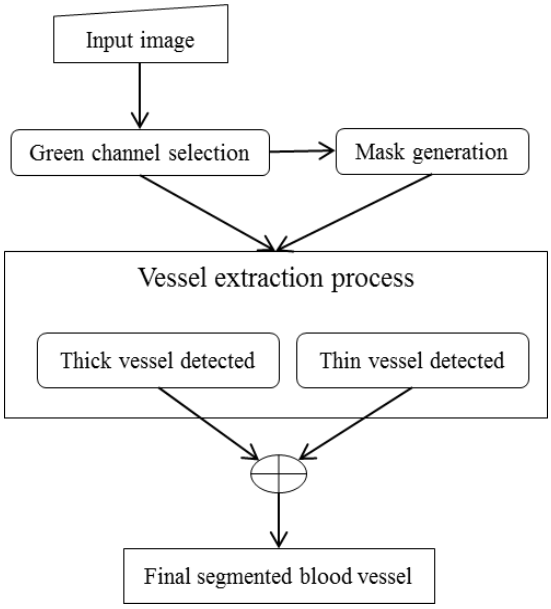

Figure 20. Overall process of Matched filter based blood vessel segmentation.

Depending upon the values passed as arguments, two different sized vessels, thick and thin, are generated. The parameter values used for thick vessel detection are σ=1.5, *yLength*=9, number of orientation (Θ)=12, *c_value*=2.3 and threshold for regionprops = 30. Whereas, for thin vessel detection, all the other parameter values are same except σ and *yLength*, which are σ =1 and *yLength*= 4.

For each orientation, first a matched filter kernel and secondly the first order derivative of Gaussian filter kernel are produced. Both type of kernels is used for convolution with the retinal image to generate matched filtered (MF) response and first order derivative of Gaussian filter (FDOG) response. Since 12 different orientations are used, 12 different results are obtained for each type of kernel. The results are stacked into 12 different planes and the maximum value for each pixel from those planes are selected to form the final MF and FDOG responses. The mean value of the matched

filter (MF) response is multiplied with *c_value* to get the threshold reference (T_c) as in Eq. (36), whereas the first order derivative of Gaussian filter (FDOG) response is filtered with mean filter of window size 31×31.

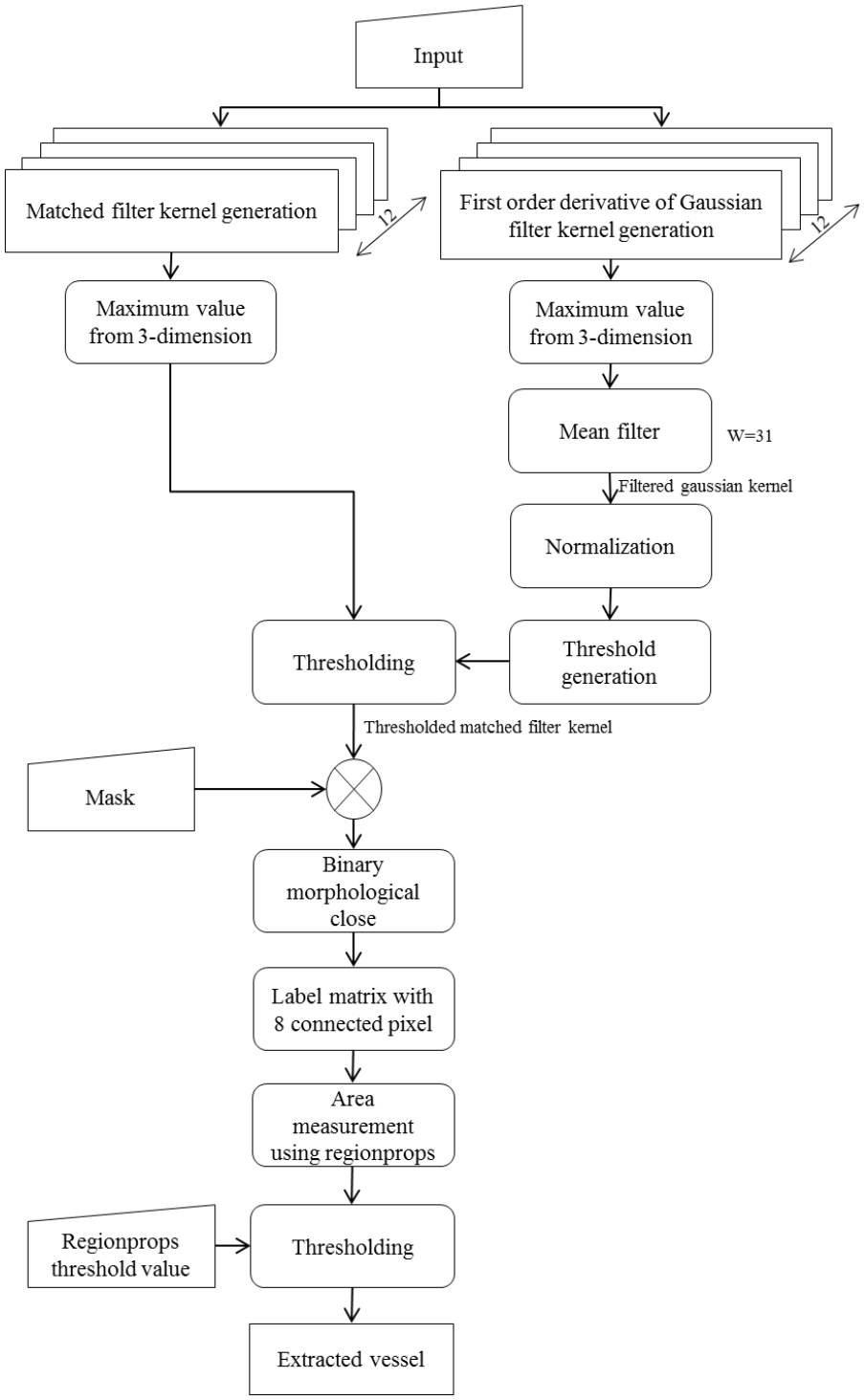

Figure 21. Detailed process diagram for blood vessels extraction block in Figure 20.

The normalized FDOG response and threshold reference (T_c) are used to generate the actual threshold value (T) as in Eq. (35). The threshold value (T) is used for thresholding the matched filter response to detect the blood vessels from a retinal image. The overall process for extracting blood vessels is illustrated in Figure 21.

The extracted blood vessels in Figure 21 are passed to the post processing block in order to obtain the final segmented image. During this process, the image is processed using morphological closing with structuring element square (3×3 pixels) followed by morphological closing on the binary image. The result is further processed by labeling the connected components with a connectivity size of 8 pixels, and by calculating the 'area' property of the image region, which specifies the actual number of pixels in the region. Finally, the threshold value for *regionprops* (which measures properties of image regions) is used for thresholding the 'area' property to get the processed image. If the region's pixel count is greater than the threshold value, then it is labeled as a vessel.

The above processes were applied separately, with different parameters, for detecting thick and thin vessels. The obtained images were combined using logical OR operation to generate the final segmented blood vessels. Along with the segmented vessels, the performance measures of the algorithm were determined by calculating the accuracy, true positive rate (*TPR*) and false positive rate (*FPR*). *TPR* and *FPR* are equivalent to sensitivity (*Se*) and specificity (*Sp*) as mentioned in Table I. The matlab code for calculating performance measure is listed in Appendix D.

During implementation, the application is divided into three functional blocks; one for generating matched and Gaussian filter kernels, another for detecting blood vessels and third for measuring performance. The varying parameters are passed to the function, which detects blood vessels, in order to generate thick and thin vessels independently. Only the values for sigma (σ), yLength (L), and constant (c) are varied, while other parameters are unchanged while detecting thick and thin vessels for particular retinal image. The base values for thick vessels detection are σ =1.5, L=9, and c=2.3 and for thin one are σ=1, L=4 and c=2.3. Changing the value of c affects the TPR and FPR but there is no significant difference in accuracy. That is, increasing c

value over 2.3 reduces *TPR* and *FPR*, while decreasing don't have adverse effect. And, small increase or decrease in σ and L value for thick and thin vessels detection, slightly reduces the performance measures.

4 Results

The implemented applications were tested using retinal images from publically available databases: DRIVE and STARE; and the results were compared against the corresponding ground truth images to calculate the performance measures of the algorithms. The algorithms for supervised and unsupervised methods of vessel segmentation were evaluated in terms of sensitivity (*Se*), specificity (*Sp*), positive predictive value (*Ppv*), negative predictive value (*Npv*), and accuracy (*Acc*) [8]. The matched filter algorithm was evaluated in terms of accuracy (*Acc*), true positive rate(*TPR*) and false positive rate(*FPR*) [20]. The formulas used for calculating these performance measures are listed in Tables I and II.

The computing system used for running all the applications was a PC with Intel core i5, 2.6 GHz CPU with 4GB RAM and 1GB of dedicated GPU.

A. Supervised method using gray-level and moment invariant based features with Neural network

The results obtained for the supervised method of vessel segmentation using gray-level and moment invariants-based features are listed in Table III and IV.

Table III. Performance results on DRIVE database images (Supervised method using gray-level and moment invariants-based features).

Image	Se	Sp	Ppv	Npv	Acc
1	**0.7445**	0.9547	0.6168	0.9744	0.9359
2	0.7292	0.9671	0.7167	0.9690	0.9427
3	0.6798	0.9608	0.6574	0.9644	0.9328
4	0.6580	**0.9785**	**0.7560**	0.9658	**0.9490**
5	0.6424	0.9738	0.7169	0.9634	0.9427
6	0.5453	0.9657	0.6319	**0.9517**	0.9248
7	0.6542	0.9760	0.7328	0.9656	0.9466
8	0.6404	0.9697	0.6653	0.9663	0.9413
9	0.5446	0.9638	0.5700	0.9600	0.9298
10	0.7017	0.9661	0.6501	0.9731	0.9444
11	0.6462	0.9685	0.6684	0.9653	0.9396
12	0.6618	0.9605	0.6127	0.9678	0.9347
13	0.6267	0.9636	0.6510	0.9597	0.9307
14	0.5896	**0.9478**	0.4985	0.9633	**0.9189**
15	0.6108	0.9501	**0.4852**	0.9694	0.9258
16	0.6172	0.9570	0.5875	0.9618	0.9363
17	**0.5205**	0.9602	0.5465	0.9560	0.9231
18	0.6363	0.9574	0.5623	0.9683	0.9319
19	0.6786	0.9556	0.5801	0.9705	0.9326
20	0.6945	0.9546	0.5484	**0.9752**	0.9355
Average	**0.6411**	**0.9625**	**0.6227**	**0.9655**	**0.9349**

Table IV. Performance results on STARE database images (Supervised method using gray-level and moment invariants-based features).

Image	Se	Sp	Ppv	Npv	Acc
1	**0.4280**	0.9626	0.4980	0.9510	0.9199
2	0.5168	0.9598	0.4784	0.9653	0.9303
3	0.7525	0.9440	0.4609	**0.9836**	0.9325
4	0.4570	0.9604	0.4805	0.9567	0.9231
5	0.7059	**0.9370**	0.5265	0.9698	0.9161
44	0.5804	0.9624	0.5358	0.9684	0.9357
77	0.7496	0.9671	0.6653	0.9779	0.9497
81	0.6017	0.9761	0.6698	0.9681	0.9481
82	0.7642	0.9629	0.6376	0.9795	0.9473
139	0.5615	0.9698	0.6189	0.9620	0.9369
162	0.6420	0.9724	0.6409	0.9725	0.9489
163	**0.7690**	0.9717	0.6948	0.9805	**0.9560**
236	0.6326	**0.9842**	**0.7990**	0.9642	0.9523
239	0.7100	0.9413	0.5336	0.9717	0.9214
240	0.4427	0.9626	0.5738	**0.9382**	**0.9095**
255	0.6327	0.9755	0.7176	0.9643	0.9448
291	0.6847	0.9510	0.4265	0.9826	0.9375
319	0.5997	0.9545	**0.3724**	0.9815	0.9392
324	0.4760	0.9539	0.4248	0.9622	0.9220
Average	**0.6162**	**0.9615**	**0.5661**	**0.9684**	**0.9353**

For training the neural network, image 27 from the training set of DRIVE images was used. Whereas for the STARE database, image 255 was used. The original authors' implementation of the algorithm used one input, three hidden layers each with 15 nodes and one output layer for both databases. In this thesis, one input, one hidden layer and one output layer were used. A neural network using the authors' original configuration was also implemented, but the results were found to be poorer than with the new configuration. New configurations were chosen for both databases with the varying number of nodes in the hidden layer. For the DRIVE images, training is done with 20 nodes in a hidden layer, while for the STARE images, training was done with 15 nodes. The training took around 25 minutes while simulation or testing required only 5 seconds to execute. For the DRIVE database, smaller amounts of nodes (e.g., 10 and 15) gave poorer classification accuracies and sensitivities than 20 nodes, which gave optimal performance results. Similarly, for STARE images, hidden layer with 10 and 20 nodes were tested but the optimal results were obtained using 15 nodes in hidden layer.

The performance results shown in Tables III and IV were obtained by applying the same threshold value *Th* for all the images in the same database (for DRIVE, 0.53 and for STARE, 0.43 were used). These threshold values are different than the values used by the original author, which were 0.63 and 0.91 for DRIVE and STARE images, respectively. When comparing with the original author's results, the implemented algorithm gives nearly same accuracy, specificity and negative predictive value (see Table V). The sensitivity and positive predictive value are smaller than original author's result. The implemented algorithm has slightly lower capability to detect thin vessels, which might be the reason for obtaining smaller values for *Se* and *Ppv*. The use of only one hidden layer rather than three layers in the neural network might explain the results obtained.

Table V. Comparison of performance results with original author (Supervised method using gray-level and moment invariants-based features).

Results	**Se**	**Sp**	**Ppv**	**Npv**	**Acc**
Original author	0.7005	0.9810	0.8330	0.9620	0.9489
Our application	0.6286	0.9620	0.5944	0.9669	0.9351

Examples of output images obtained from the implemented application (Supervised method) for DRIVE and STARE images are shown in Figures 22 and 23, respectively.

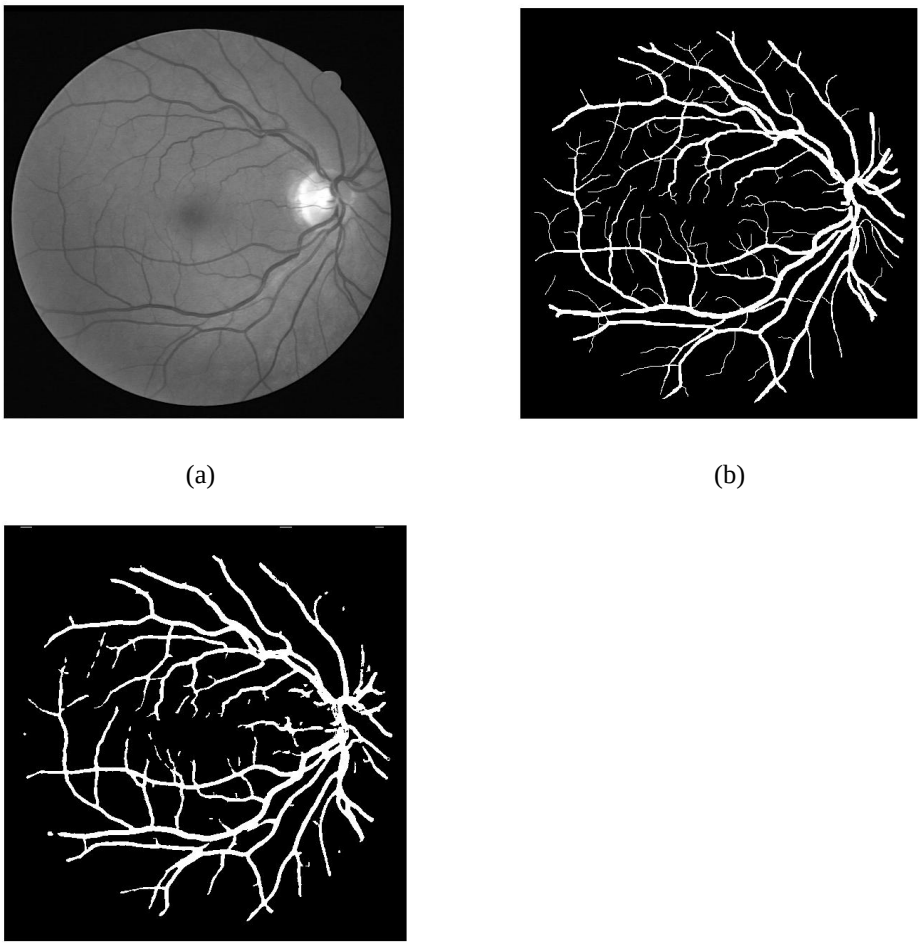

(a) (b)

(c)

Figure 22. (a) Original green channel image (DRIVE database image 1, [36]) (b) The ground truth image, (c) The extracted vessels image from supervised method using gray-level and moment invariants-based features.

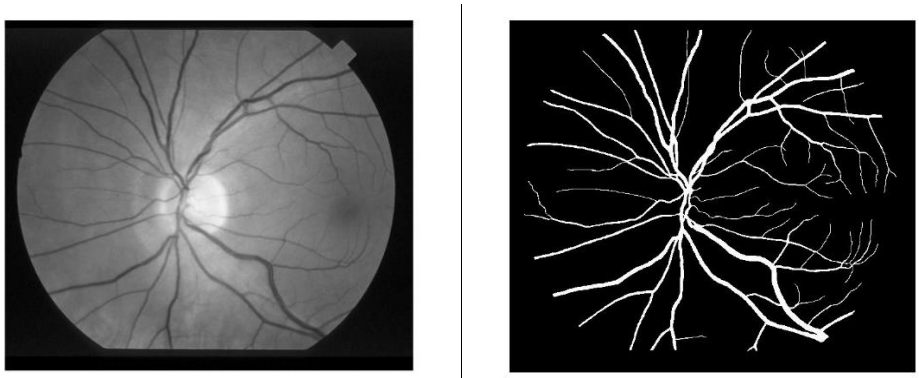

(a) (b)

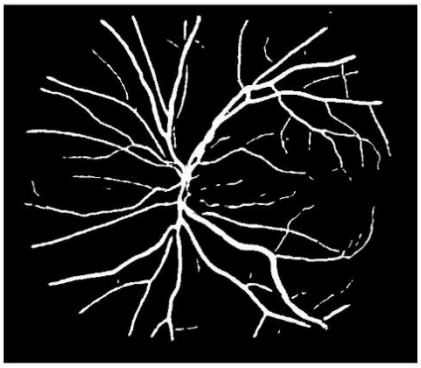

(c)

Figure 23. (a) Original green channel image (STARE database image 82 [37]), (b) The ground truth image, (c) The extracted vessels image from supervised method using gray-level and moment invariants-based features.

From Figures 22 and 23, one can clearly see that the implementation of the algorithm is able to detect thick vessels relatively well. Method used is not as efficient in detecting thin vessels, which leads to lower sensitivity. The computational time required to process a single image and extract seven features is approximately 2.5 minutes while executing a test required only 5 seconds. The author's implementation took only 1.5 minutes, which is faster than the application being implemented. This might be due the difference in implementation procedure for the feature extraction process.

B. Unsupervised method using local entropy and co-occurrence matrix

The performance results obtained by executing the implementation of unsupervised method of vessel segmentation using local entropy and co-occurrence matrix are listed in Tables VI and VII.

Table VI. Performance results on DRIVE database images (Unsupervised method using local entropy and co-occurrence matrix).

Image	Se	Sp	Ppv	Npv	Acc
1	0.7221	0.9851	0.8252	0.9731	0.9616
2	0.7418	0.9826	0.8291	0.9708	0.9579
3	0.5531	0.9918	0.8829	**0.9524**	0.9481
4	0.6883	0.9842	0.8155	0.9689	0.9570
5	0.5592	**0.9946**	**0.9146**	0.9562	0.9538
6	**0.5435**	0.9934	0.8993	0.9527	0.9496
7	0.6591	0.9793	0.7620	0.9662	0.9501
8	0.5558	0.9805	0.7281	0.9591	**0.9439**
9	0.5484	0.9920	0.8577	0.9614	0.9560
10	0.5950	0.9916	0.8643	0.9647	0.9590
11	0.6838	**0.9662**	0.7386	0.9691	0.9510
12	0.6254	0.9883	0.8343	0.9654	0.9569
13	0.6110	0.9895	0.8633	0.9591	0.9525
14	0.6944	0.9813	0.7660	0.9733	0.9581
15	**0.7575**	0.9712	**0.6693**	**0.9811**	0.9559
16	0.6516	0.9879	0.8425	0.9662	0.9575
17	0.6225	0.9849	0.7919	0.9659	0.9543
18	0.7028	0.9848	0.7993	0.9747	0.9625
19	0.7219	0.9923	0.8945	0.9753	**0.9699**
20	0.6379	0.9880	0.8087	0.9717	0.9623
Average	**0.6438**	**0.9855**	**0.8194**	**0.9664**	**0.9559**

Table VII. Performance results on STARE database images (Unsupervised method using local entropy and co-occurrence matrix).

Image	Se	Sp	Ppv	Npv	Acc
1	0.6484	0.9504	0.5314	0.9689	0.9263
2	0.5301	0.9522	0.4417	0.9661	0.9241
3	0.8477	**0.8911**	**0.3313**	0.9892	**0.8885**
4	**0.2782**	**0.9973**	**0.8908**	0.9452	0.9441
5	0.7950	0.9434	0.5822	0.9789	0.9301
44	0.8684	0.9188	0.4448	0.9894	0.9153
77	0.8819	0.9578	0.6453	0.9894	0.9517
81	0.7849	0.9655	0.6471	0.9823	0.9520
82	0.8515	0.9720	0.7220	0.9871	0.9625
139	0.8079	0.9514	0.5922	0.9826	0.9398
162	0.8433	0.9678	0.6676	0.9877	0.9589
163	**0.9041**	0.9694	0.7121	**0.9918**	0.9643
235	0.8037	0.9728	0.7431	0.9807	0.9578
236	0.7929	0.9749	0.7590	0.9793	0.9584
239	0.7179	0.9733	0.7172	0.9732	0.9511
240	0.4685	0.9885	0.8223	**0.9424**	0.9354
255	0.6950	0.9862	0.8324	0.9705	0.9602
291	0.5448	0.9904	0.7512	0.9761	0.9679
319	0.6084	0.9877	0.6902	0.9825	**0.9714**
324	0.5424	0.9830	0.6951	0.9678	0.9536
Average	**0.7110**	**0.9647**	**0.6610**	**0.9766**	**0.9457**

The performance results in Tables VI and VII were obtained by generating mask with threshold value greater than 20/255 for DRIVE database images, while value greater than 35/255 for STARE database images was used. The matched filter response was generated with same parameters (σ = 1.2, *yLength* = 9, and Θ = 12) for both databases. These values generated the best results, but they are not only the parameters that affect the implemented application's capability. Increasing or decreasing *yLength* value degraded the outcome of the final result. While with parameter σ, no significant difference is found when the value is changed by small amount. The overall results obtained were relatively good for most retinal images. Most of the DRIVE images are normal retinal images from healthy humans, which produced comparable results [20]. But some images of STARE database contain lesions (e.g., images 2, 3 and 4), which showed higher deviation in results than other images. Those images have relatively lower sensitivity and accuracy than others. The average results produced by the application are relatively close to the results published by the original author. Only major difference is found in '*Se*' value. Since a detailed expla-

nation of the algorithm is missing in the original paper, the implementation could have some faults, which might have resulted in lower '*Se*' value in this study. In addition, the original publication does not contain values for '*Ppv'* and '*Npv'*. Table VIII shows the comparison of the performance results between the implemented application and the original paper's results.

Table VIII. Comparison of performance results with original author (Unsupervised method using local entropy and co-occurrence matrix).

Results	**Se**	**Sp**	**Ppv**	**Npv**	**Acc**
Original author	0.9648	0.9480	NA	NA	0.9759
Our application	0.6774	0.9751	0.7402	0.9715	0.9508

Examples of output images obtained from unsupervised method's implementation for STARE and DRIVE images are shown in Figure 24 and 25, respectively.

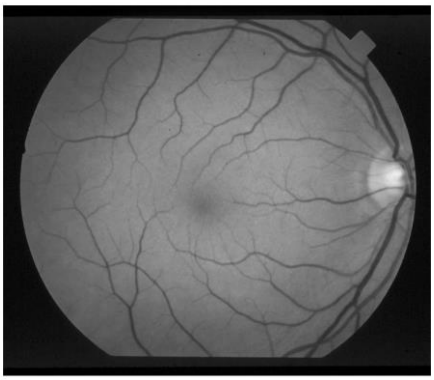

(a)

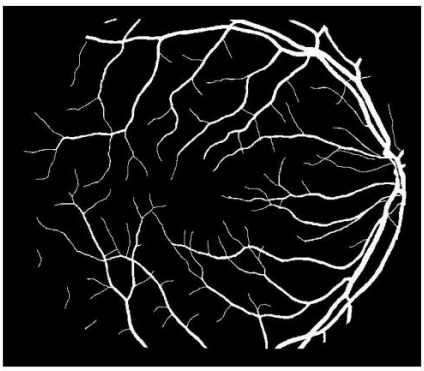

(b)

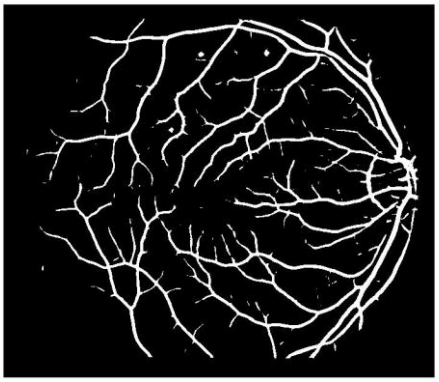

(c)

Figure 24. (a) Original green channel image (STARE image 82 [37]), (b) The ground truth image, (c) The extracted vessels image from unsupervised method using local entropy and co-occurrence matrix.

(a)

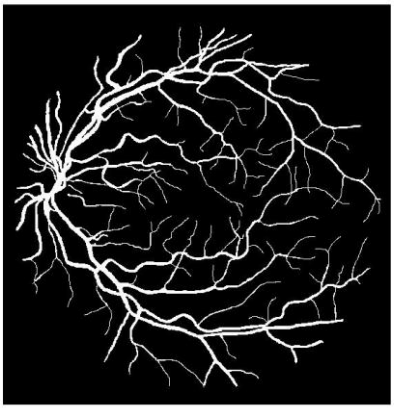

(b)

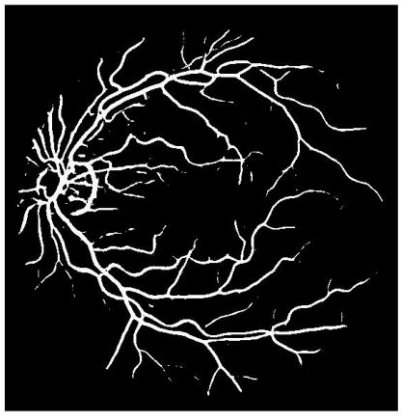

(c)

Figure 25. (a) Original green channel image (DRIVE database image 1 [36]), (b) The ground truth image, (c) The extracted vessels image from unsupervised method using local entropy and co-occurrence matrix.

The computational time required to process one image was approximately 1.5 sec for both database images, which is faster than the execution time (3 sec) required for the original author's implementation. The computer used for computations had better specifications, which could be the reason for the faster execution.

C. Matched filtering method using first order derivative of Gaussian

For the matched filter method of vessel segmentation using first order derivative, the performance measures calculated were true positive rate (*TPR*), false positive rate (*FPR*), and accuracy (*Acc*). The results obtained from this method of vessel segmentation are listed in Tables IX and X.

Table IX. Performance results for DRIVE images.

Image	TPR	FPR	Acc
1	0.6791	0.0163	0.9432
2	0.6711	0.0145	0.9378
3	0.5532	0.0158	**0.9203**
4	0.6543	0.0188	0.9365
5	0.6035	**0.0094**	0.9368
6	0.5481	0.0102	0.9261
7	0.6174	0.0171	0.9335
8	0.5504	0.0245	0.9212
9	**0.5275**	0.0099	0.9344
10	0.6601	0.0168	0.9436
11	0.6683	0.0220	0.9370
12	0.5896	0.0138	0.9354
13	0.5914	0.0144	0.9285
14	0.6360	0.0162	0.9422
15	**0.7778**	**0.0419**	0.9390
16	0.6194	0.0116	0.9389
17	0.5455	0.0134	0.9311
18	0.6542	0.0176	0.9436
19	0.7690	0.0136	**0.9595**
20	0.6960	0.0220	0.9471
Average	**0.6305**	**0.0167**	**0.9368**

Table X. Performance results for STARE images.

Image	TPR	FPR	Acc
1	0.6289	0.0648	0.9017
2	0.5694	**0.0757**	**0.8944**
3	0.7148	0.0496	0.9311
4	0.4895	0.0072	0.9440
5	0.6345	0.0263	0.9315
44	**0.8833**	0.0509	0.9451
77	0.8797	0.0341	0.9590
81	0.8450	0.0263	0.9642
82	0.8209	0.0265	0.9581
139	0.7533	0.0410	0.9366
162	0.8151	0.0283	0.9562
163	0.8449	0.0196	0.9662
235	0.7635	0.0248	0.9503
236	0.7493	0.0235	0.9492
239	0.6584	0.0163	0.9453
240	0.6209	0.0097	0.9473
255	0.7617	0.0154	0.9578
291	0.6155	**0.0049**	0.9683
319	0.6691	0.0126	**0.9687**
324	**0.4870**	0.0136	0.9400
Average	**0.7102**	**0.0285**	**0.9456**

The performance results were calculated after combining thin and thick detected retinal vessels from a same image. In order to spot thin vessels, the parameters used were σ=1, L=4 and c=2.3 while for thick vessels, the values were σ=1.5, L=9, and

c=2.3. If these values were increased or decreased, the results became slightly poorer. While increasing the value of c, TPR and FPR lowers but the accuracy is not affected. For example; when the value of c is changed to 2.5, the accuracy is about 0.947 while TPR and FPR are 0.6401 and 0.0210, respectively. For c=2.7, the performance results, in general, are Acc=0.941, TPR=0.6117, FPR=0.0192. When σ and L values are slightly increased or decreased, the performance measures are not affected.

The output images obtained for DRIVE and STARE images are shown in Figures 26 and 27, respectively.

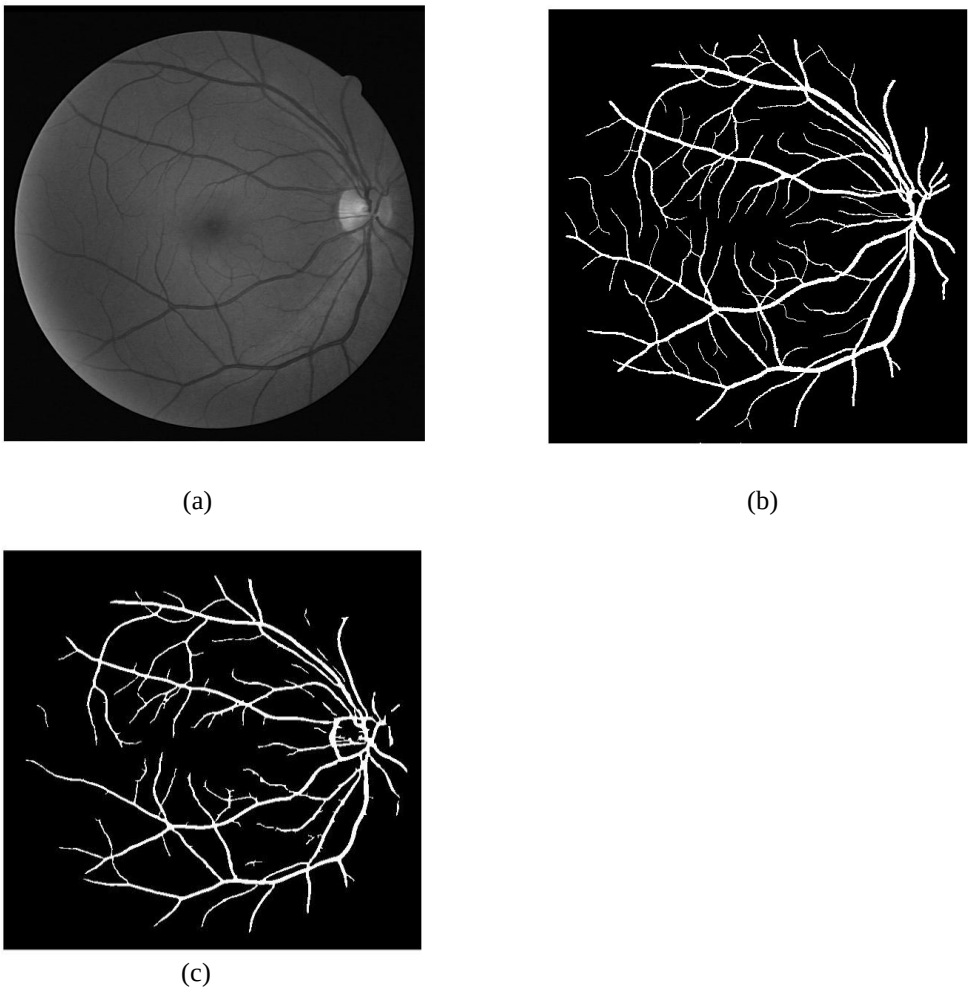

(a) (b)

(c)

Figure 26. (a) Original green channel image (DRIVE database image 19 [36]), (b) The ground truth image, (c) The extracted vessels image from matched filter method using first order derivative of Gaussian.

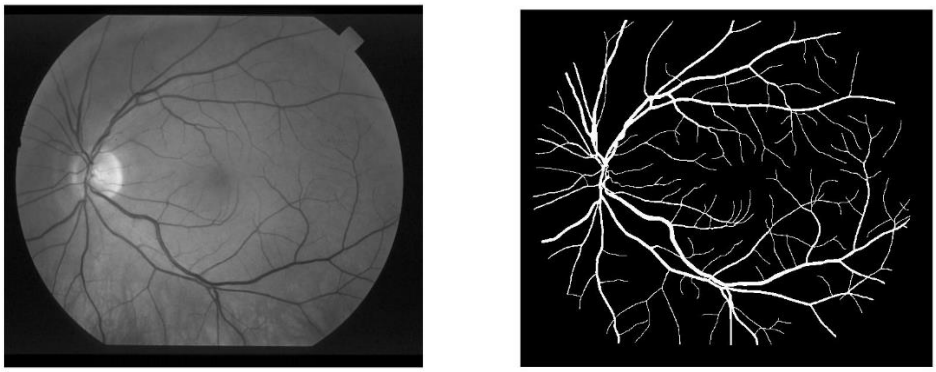

(a) (b)

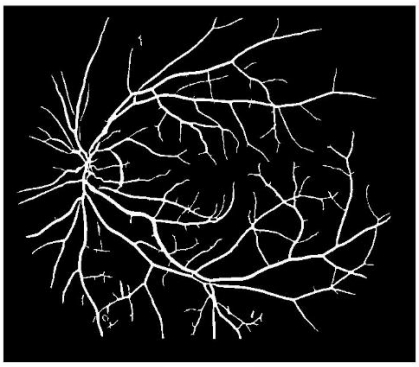

(c)

Figure 27. (a) Original green channel image (STARE image 162 [37]), (b) The ground truth image, (c) The extracted vessels image from matched filter method using first order derivative of Gaussian.

While comparing the results with those of the original author, the accuracy is almost same but TPR and FPR have slight differences (see Table XI). The correctly classified vessel pixels' percent is nearly 4% smaller than the authors' result while falsely classified vessel pixels' is 1% smaller. This shows the implementation performs almost as well in detecting non-vessels while is poorer in detecting correct vessel pixels than the original author's implementation.

Table XI. Comparison of performance results with original author (Matched filter method using first order derivative of Gaussian).

Results	TPR	FPR	Acc
Original author	0.7143	0.0301	0.9410
Our application	0.6703	0.0226	0.9412

The computational time required was about 1.5 sec to process one image for both database images, which was faster than the execution time (10 sec) required for the original author's implementation.

Some vessel segmented images obtained from three different implemented algorithms are listed in Appendix A.

5 Conclusion

In this thesis, the literatures regarding different methods for retinal blood vessel segmentation were studied and three different state-of-the-art methods were implemented [8, 12, 20]. Based on the study of literature and selection of three different methods, the issues addressed in this thesis are: 1) How accurate are the selected blood vessel segmentation methods in extracting blood vessels from fundus images, and 2) Are results from automated blood vessel extraction systems trustworthy compared to manual segmentations done by experts.

There are different types of blood vessel segmentation algorithms available which are mentioned in chapter 2. To test and evaluate the algorithms, fundus images are needed. Hence, the publicly available image databases STARE and DRIVE play an important role for evaluating and measuring the performance of algorithms, which are presented in chapter 2. These databases contain fundus images for training and testing algorithms including the corresponding ground truth images. Due to its availability for general public, the study and performance estimation of vessel segmentation algorithms has become easy. In this thesis, the three state-of-the-art methods [8, 12, 20] from three different categories (i.e. supervised, unsupervised, and match filtering methods) were selected based on their good performance results as published in the literature. The individual methods were studied in detail and described in chapter 2.

Among the three state-of-the-art methods, the literature related to the supervised method [8] and matched filtering based method [12] are well documented, which made the implementation process easier. Whereas the unsupervised method [20] is relatively poorly documented, so other similar kind of literature [69, 70] was taken into consideration for studying and implementing the algorithm.

For supervised method based algorithm, the performance results are better for DRIVE database images than for STARE (see Table III and IV). When the overall results are compared with the state-of-the-art method's results, the algorithm has

lower performance results which are illustrated in Table V. The possible reasons could be due to difference in neural network design and selection of different threshold values than used in the original publication. When NN was trained with three hidden layers, each having 15 neurons as in the original literature, the results were relatively poor. So a new NN was designed with one hidden layer containing 15 neurons, which produced slightly better performance results. According to the original literature, the threshold values of 0.63 and 0.91 were used for DRIVE and STARE database images, respectively. The algorithm implemented in this thesis used values of 0.53 and 0.43 for DRIVE and STARE, respectively, as those threshold values generated the optimal results.

For unsupervised method based algorithm, the sensitivity values for STARE database images are better than for DRIVE, while positive predictive values (*Ppv*) for DRIVE database images are better than for STARE. Other performance measures are nearly the same for both image databases (see Table VI and VII). The overall results obtained from algorithm are lower than the ones in the original publication which are shown in Table VIII. The accuracy and specificity are nearly the same, but the implemented algorithm's sensitivity is relatively low compared to the original result. Since the literature is hard to understand due to its poor documentation, the algorithm's details could have been misunderstood, for example, in the cases of GLCM calculation and JRE thresholding. This could be the main reason for obtaining lower results from the algorithm. The literature lacks explanation about parameters' values used for evaluating the algorithm and also the results; positive predictive value *(Ppv)* and negative predictive value *(Npv)* (see Table VIII). Moreover, the matched filter based algorithm's results are nearly the same with slightly better true positive rate (*TPR*) for DRIVE database images. When the algorithm's results are compared to the state-of-the-art method's results, the implemented algorithm has lower *TPR* while other measures are in close approximation, which are shown in Table XI.

After analyzing the results of three different algorithms, it is found that the performance results of state-of-the-art methods are better than the results of the implemented algorithms. Furthermore, the images with high level of lesions have poorer per-

formance results than the normal retinal images. Although the accuracy of all three methods is nearly the same when compared with the corresponding state-of-the-art methods, the distinguishing characteristic (i.e., lower sensitivity value) is found in the all implemented algorithms. This has affected the determination of the amount of correctly classified vessel pixels. Hence, the true vessel detection rate is lower. However, the algorithms have high accuracy (i.e., more than 93 percent for all methods), which could be the key factor for accepting the algorithms to be used for the extraction of blood vessels.

The algorithms have capability of detecting vessels and background from fundus images but only to a certain extent. As the manual segmentation of blood vessels is hard and time consuming, it would be better to use a fast, automated system which could detect higher amount of blood vessels. Besides saving time, it could decrease the number of experts required and increase the ability to segment large numbers of fundus images in a short period of time. Since the currently implemented algorithms have relatively low correctly classified vessel rates, they are not feasible for implementation into automatized system. Although the accuracy rate of algorithms is reasonable, improvement in the true vessel and background detection should be done. Hence, the automated vessel detection system is not fully trustworthy with the results being achieved.

There are few areas for improving the algorithms' performance. The algorithms were evaluated using only DRIVE and STARE image databases, which might be not enough for analyzing the algorithms to full extent. So, for the evaluation of algorithms, other available image databases could be included. In addition, the noise in fundus image usually lowers the overall results, if it is not handled properly. Hence, other preprocessing and post-processing strategies could be included along with the existing ones in order to improve the overall performance results. The study of these subjects is considered to be important for the future research.

References

[1] Soares J.V., Leandro J.J., Cesar R.M., Jelinek H.F., Cree M.J., (2006): Retinal vessel segmentation using the 2-D Gabor wavelet and supervised classification. *IEEE Transaction of Medical Imaging*, vol.25, pp.1214–1222.

[2] Fathi A., Naghsh-Nilchi A.R. (2012): Automatic wavelet-based retinal blood vessels segmentation and vessel diameter estimation. *Biomedical Signal Processing and Control*, vol.8(1), pp.71-80.

[3] Fang B., Hsu W., Lee M.U., (2003): On the Detection of Retinal Vessels in Fundus Images. http://hdl.handle.net/1721.1/3675 (04.05.2016)

[4] You X., Peng Q., Yuan Y., Cheung Y., Lei J. (2011): Segmentation of retinal blood vessels using the radial projection and semi-supervised approach. *Pattern Recognition*, vol.44, pp.2314-2324.

[5] Wasan B., Cerutti A., Ford S., Marsh R., (1995): Vascular network changes in the retina with age and hypertension. *Journal of Hypertension*, vol.13(12), pp.1724-1728.

[6] Sussman E.J., Tsiaras W.G., Soper K.A., (1982): Diagnosis of diabetic eye disease. *The Journal of the American Medical Association*, vol.247(23), pp.3231-3234.

[7] Nguyen U.T., Bhuiyan A., Park L.A., Ramamohanarao K., (2013): An effective retinal blood vessel segmentation method using multi-scale line detection. *Pattern Recognition*, vol.46, pp.703-715.

[8] Diego M., Arturo A., Manuel E., and Jose M. (2011): A new supervised method for blood vessel segmentation in retinal images by using gray-level and moment invariants-based features. *IEEE Transactions on Medical Imaging*, vol.30(1), pp.146-158.

[9] Ricci E., Perfetti R., (2007): Retinal blood vessel segmentation using line operators and support vector classification. *IEEE Transaction of Medical Imaging*, vol.26, pp.1357–1365.

[10] Staal J., Abramoff M.D., Niemeijer M., Viergever M.A., Ginneken B., (2004): Ridge-based vessel segmentation in color images of the retina. IEEE Transactions on Medical Imaging, vol.23, pp.501-509.

[11] Sinthanayothin C., Boyce J., Williamson C.T., (1999): Automated localisation of the optic disk, fovea, and retinal blood vessels from digital colour fundus images. *The British Journal of Ophthalmology*, vol.83(8), pp.902-910.

[12] Villalobos-Castaldi F.M., Felipe-Riveron E.M., Sanchez-Fernandez L.P., (2010): A fast, efficient and automated method to extract vessels from fundus images. *Journal of Visualization*, vol.13, pp.263-270.

[13] Kande G.B., Subbaiah P.V., Savithri T.S., (2009): Unsupervised fuzzy based vessel segmentation in pathological digital fundus images. *Journal of Medical Systems*, vol.34, pp.849-858.

[14] Rahebi J., Hardalac F., (2014): Retinal Blood Vessel Segmentation with Neural Network by Using Gray-Level Co-Occurrence Matrix-Based Features. *Journal of Medical Systems*, vol.38(8), pp.85-97.

[15] Tolias Y., Panas S., (1998): A fuzzy vessel tracking algorithm for retinal images based on fuzzy clustering. *IEEE Transactions on Medical Imaging*, vol.17(2), pp.263-273.

[16] Al-Rawi M., Qutaishat M., Arrar M. (2006): An improved matched filter for blood vessel detection of digital retinal images. *Computers in Biology and Medicine*, vol.37, pp.262-267.

[17] Chaudhuri S., Chatterjee S., Katz N., Nelson M., and Goldbaum M. (1989): Detection of blood vessels in retinal images using two-dimensional matched filters. *IEEE Transaction on Medical Imaging*, vol.8, pp.263–269.

[18] Zolfagharnasab H., Naghsh-Nilchi A.R. (2014): Cauchy based matched filter for retinal vessels detection. *Journal of Medical Signals and Sensors*, vol.4(1), pp. 1-9.

[19] Hoover A., Kouznetsova V., Goldbaum M. (2000): Locating blood vessels in retinal images by piecewise threshold probing of a matched filter response. *IEEE Transaction on Medical Imaging*, vol.19(3), pp.203-210.

[20] Zhang B., Zhang L., Karray F., (2010): Retinal vessel extraction by matched filter with first-order derivative of Gaussian. *Computers in Biology and Medicine*, vol.40, pp.438-445.

[21] Fraz M.M., Remagnino P., Hoppe A., Uyyanonvara B., Rudnicka A., Owen C., Barman S. (2012): Blood vessel segmentation methodologies in retinal images – A survey. *Computer Methods and Programs in Biomedicine*, vol.108, pp. 407-433.

[22] Sun K., Chen Z., Jiang S., Wang Y. (2011): Morphological multiscale enhancement, fuzzy filter and watershed for vascular tree extraction in angiogram. *Journal of Medical Systems*, vol.35(5), pp.811-824.

[23] Mookiah M.R., Acharya U.R., Chua C.K., Lim C.M., Laude A. (2013): Computer-aided diagnosis of diabetic retinopathy: A review. *Computers in Biology and Medicine*, vol.43, pp.2136-2155.

[24] Al-Diri B., Hunter A., Steel D., (2009): An active contour model for segmenting and measuring retinal vessels. *IEEE Transactions on Medical Imaging*, vol.28(9), pp.1488-1497.

[25] Al-Diri B., Hunter A., Steel D. (2009): An active contour model for segmenting and measuring retinal vessels. *IEEE Transactions of Medical Imaging*, vol.38(9), pp.1488-1497.

[26] Lam B.S., Gao Y., Liew A.W. (2010): General retinal vessel segmentation using regularization based multiconcavity modeling. *IEEE Transactions of Medical Imaging*, vol.29, pp.1369-1381.

[27] Sum K.W., Cheung P.Y., (2008): Vessel extraction under non-uniform illumination: a level set approach. *IEEE Transactions on Biomedical Engineering*, vol.55(1), pp.1196-1204.

[28] Osareh A., Shadgar B., (2009): Automatic blood vessel segmentation in color images of retina. *Iranian Journal of Science and Technology*, vol.33, pp.191–206.

[29] Mendonça A.M., Campilho A., (2006): Segmentation of retinal blood vessels by combining the detection of centerlines and morphological reconstruction. *IEEE Transaction on Medical Imaging*, vol.25(9), pp.1200-1213.

[30] Taylor H.R., Keeffe J.E., (2001): World blindness: A 21st century perspective. *British Journal of Ophthalmology*, vol.85, pp.261-266.

[31] Human eye anatomy: http://www.allaboutvision.com/resources/anatomy.htm (02.05.2016)

[32] Human eye: http://www.nkcf.org/how-the-human-eye-works/ (02.05.2016)

[33] Human eye diagram: https://nei.nih.gov/health/eyediagram (02.05.2016)

[34] Macula background: http://patient.info/doctor/macular-disorders (03.05.2016)

[35] Montgomery T.: Macula. http://www.tedmontgomery.com/the_eye/macula.html (03.05.2016)

[36] Research Section, Digital Image for Vessel Extraction (DRIVE) Database. Utrecht, The Netherlands, Univ. Med. Center Utrecht, Image Sci. Inst. http://www.isi.uu.nl/Research/Databases/DRIVE/, (05.01.2016)

[37] STARE Project Website. Clemson, SC, Clemson University. http://www.ces.clemson.edu/~ahoover/stare/, (12.01.2016)

[38] Frangi A.F., Niessen W.J., Vincken K.L., Viergever M.A., William W., Alan C., Scott D. (1998): Mulitscale vessel enhancement filtering. *Medical Image Computing and Computer-Assisted Interventation*, vol.1497, pp.130-137.

[39] Miri M.S., Mahloojifar A. (2011): Retinal image analysis using curvelet transform and multistructure elements morphology by reconstruction. *IEEE Transactions on Biomedical Engineering*, vol.58, pp.1183-1192.

[40] Sato Y., Araki T., Hanayama M., Naito H., Tamura S. (1998): A viewpoint determination system for stenosis diagnosis and quantification in coronary angiographic image acquisition. *IEEE Transactions of Medical Imaging*, vol.17(1), pp.121-137.

[41] Chua L.O., Yang L. (1988): Cellular neural networks. *Transaction of Circuits and Systems*, vol.35, pp.1257-1272.

[42] Alonso-Montes C., Vilario D.L., Dudek P., Penedo M.G., (2008): Fast retinal vessel tree extraction: a pixel parallel approach. *International Journal of Circuit Theory and Applications*, vol.36, pp.641-651.

[43] Pattern recognition. http://www.mathworks.com/discovery/pattern-recognition.html (07.04.2016)

[44] Pattern recognition. http://global.britannica.com/technology/pattern-recognition-computer-science (07.04.2016)

[45] Aksoy S. (2015): Introduction to pattern recognition http://www.cs.bilkent.edu.tr/~saksoy/courses/cs551/slides/cs551_intro.pdf (08.04.2016)

[46] Dukart J., (2015): Basic Concepts of Image Classification Algorithms Applied to Study Neurodegenerative Diseases. *Brain Mapping: An Encyclopedic Reference*, vol.3, pp.641-646.

[47] Sathya R., Abraham A., (2013): Comparison of Supervised and Unsupervised Learning Algorithms for Pattern Classification. *International Journal of Advanced Research in Artificial Intelligence*, vol.2(3), pp.34-38.

[48] DongMel C. and Douglas S., (2002): The Effect of Training Strategies on Supervised Classification at Different Spatial Resolutions. *Photogrammetric Engineering & Remote Sensing*, vol.68(11), pp.1155-1161.

[49] Joao V.S., Jorge J.G., Roberto M.C., Herbert F.J., Michael J.C., (2006): Retinal Vessel Segmentation Using the 2-D Gabor Wavelet and Supervised Classification. *IEEE Transaction of Medical Imaging*, vol.25, pp.1214-1222.

[50] Elisa R., Renzo P., (2007): Retinal Blood Vessel Segmentation Using Line Operators and Support Vector Classification. *IEEE Transaction of Medical Imaging*, vol.26, pp.1357-1365.

[51] Ahuja N., RosenFeld A., Haralick R.M., (1980): Neighbor gray levels as features in pixel classification. *Pattern Recognition*, vol.12, pp.251-260.

[52] Rocha L., Velho L., Carvalho P.: Image Moments-Based Structuring and Tracking of Objects. Instituto Nacional de Matematica Pura e Aplicada. http://sibgrapi.sid.inpe.br/col/sid.inpe.br/banon/2002/10.23.11.34/doc/35.pdf (08.04.2016)

[53] Walter T., Massin P., Erginay A., Ordonez R., Jeulin C., Klein J.C., (2007): Automatic detection of microaneurysms in color fundus images. *Medical Image Analysis*, vol.11, pp.555-566.

[54] Top hat transformation. http://www.mathworks.com/help/images/ref/imtophat.html (08.04.2016)

[55] Kumar G., (2014): A Detailed Review of Feature Extraction in Image Processing Systems. *Fourth International Conference on Advanced Computing & Communication Technologies,* pp.5-12.

[56] Han Z., Yin Y., Meng X., Yang G., and Yan X., (2014): Blood vessel segmentation in pathological retinal image. *IEEE International Conference on Data Mining Workshop,* pp.960-967.

[57] Flusser and Suk. T., (2006): Rotation Moment Invariants for Recognition of Symmetric Objects. *IEEE Transactions on Image Processing,* vol.15, pp.3784-3790.

[58] Dominguez S., (2013): Image analysis by moment invariants using a set of step-like basis functions. *Pattern Recognition Letter,* vol.34(16), pp.2065–2070.

[59] Huang Z., & Leng J., (2010): Analysis of Hu's Moment Invariants on Image Scaling and Rotation. *International Conference on Computer Engineering and Technology*, vol.7, pp.476-480.

[60] Caudill M., (1987): Neural Network Primer: Part I. *AI Expert,* vol.2(12), pp.46-52.

[61] Neural network. http://pages.cs.wisc.edu/~bolo/shipyard/neural/local.html. (10.04.2016).

[62] Huang G.B., Chen Y.Q., Babri H.A., (2000): Classification ability of single hidden layer feedforward neural networks. *IEEE Transaction on Neural Network,* vol.11, pp.799–801.

[63] Kun J. (2012): Backpropagation algorithm. https://jeremykun.com/2012/12/09/neural-networks-and-backpropagation/ (11.04.2016).

[64] Soares J.B., Leandro J.G., Cesar R.M., Jelinek H.F., Cree M.J., (2006): Retinal vessel segmentation using the 2-D Gabor wavelet and supervised classification. *IEEE Transactions on Medical Imaging*, vol.25, pp.1214-1222.

[65] You X., Peng Q., Yuan Y., Cheung Y., Lei J., (2011): Segmentation of retinal blood vessels using the radial projection and semi-supervised approach. *Pattern Recognition,* vol.44, pp.2314-2324.

[66] Niemeijer M., Staal J.J., Ginneken B., Loog M., Abramoff M.D., (2004): Comparative study of retinal vessel segmentation methods on a new publicly available database. *SPIE Medical Imaging*, vol.5370, pp.648-656.

[67] Kohonen T., Simula O., (1996): Engineering Applications of the Self-Organizing Map. *Proceeding of the IEEE*, vol.84(10), pp.1354-1384.

[68] Unsupervised learning: http://www.economistinsights.com/technology-innovation/opinion/%E2%80%9Cunsupervised-learning%E2%80%9D-and-future-analytics (03.04.2016)

[69] Yang C.W., Ma D.J, Wang C.M., Wen C.H., Le C.S., Chang C., (2000): Computer-aided diagnostic detection system of venous beading in retinal images. *Optical Engineering*, vol.39(5), pp.1293-1303.

[70] Chanwinmaluang T., Fan G., (2003): An efficient blood vessel detection algorithm for retinal images using local entropy thresholding. *International Symposium on Circuits and Systems*, vol.5, pp.21-24.

[71] Aksoy S., Haralick R.M., (1998): Textural Features for Image Database Retrieval. *Proceedings of IEEE Workshop on Content-Based Access of Image and Video Libraries*, pp.45-49.

[72] Haralick R.M., Shanmuga K., Dinstein I., (1973): Textural features for image classification. *IEEE Transaction on System, Man and Cybernetics*, vol.3(6), pp. 610-621.

[73] Gebejes A., Huertas R., (2013): Texture Characterization based on Grey-Level Co-occurrence Matrix. *Conference of Informatics and Management Sciences*, pp.375-378.

[74] Simo A., Ves E., (2001): Segmentation of macular fluorescein angiographies: A statistical approach. *Pattern Recognition*, vol.34, pp.795-809.

[75] Ng J., Clay S.T., Barman S.A., Fielder A.R., Moseley M.J., Parker K.H., Paterson C., (2010): Maximum likelihood estimation of vessel parameters from scale space analysis. *Image and Vision Computing*, vol.28(1), pp.55-63.

[76] Salem N.M., Salem S.A., and Nandi A.K., (2007): Segmentation of retinal blood vessels using a novel clustering algorithm (RACAL) with a partial supervision strategy. *Medical and Biological Engineering and Computing*, vol.45, pp.261-273.

[77] Chawimaluang T., Fan G. (2003): An effective blood vessel detection algorithm for retinal images using local entropy thresholding. *Proceeding of the 2003 International Symposium on Circuits and Systems*, vol.5, pp.21-24.

[78] Gaussian function properties: https://www.dsprelated.com/freebooks/sasp/Gaussian_Function_Properties.html (28.04.2016).

[79] Kuijper A., (2010): *Scale Space and PDE methods in image analysis and processing*. Technische Universitat Darmstadt, http://www.gris.informatik.tu-darmstadt.de/~akuijper/course/TUD11/lecture3.pdf, (29.04.2016).

[80] Cinsdikici M.G., Aydin D., (2009): Detection of blood vessels in ophthalmoscope images using MF/ant (matched filter/ant colony) algorithm. *Computer Methods and Programs in Biomedicine*, vol.96, pp.85-95.

[81] Yao C., Chen H., (2009): Automated retinal blood vessels segmentation based on simplified PCNN and fast 2D-Otsu algorithm. *Journal of Central South University of Technology*, vol.16, pp.640-646.

Appendix A: Images showing segmentation results obtained from different blood vessel segmentation algorithms

1. Supervised method

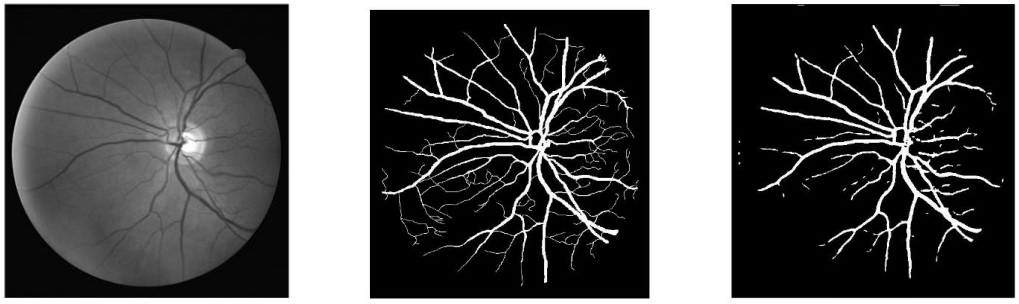

1(a) 1(b) 1(c)

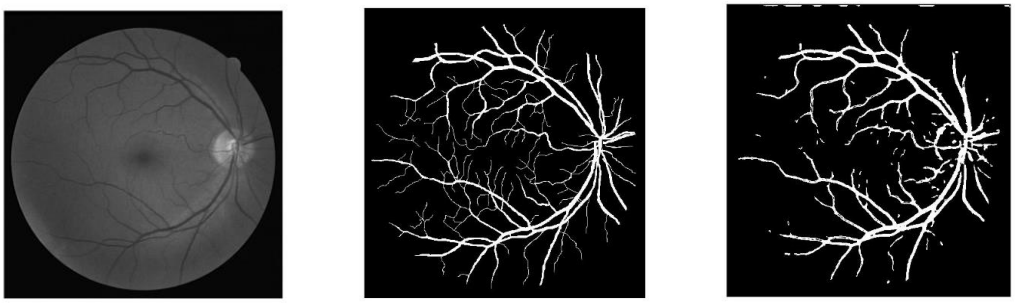

2(a) 2(b) 2(c)

Figure A.1: Figures 1 and 2 are DRIVE images 4 and 10, respectively. 1(a) and 2(a) are green channel images, 1(b) and 2(b) are ground truth images, 1(c) and 2(c) are results from supervised segmentation algorithm.

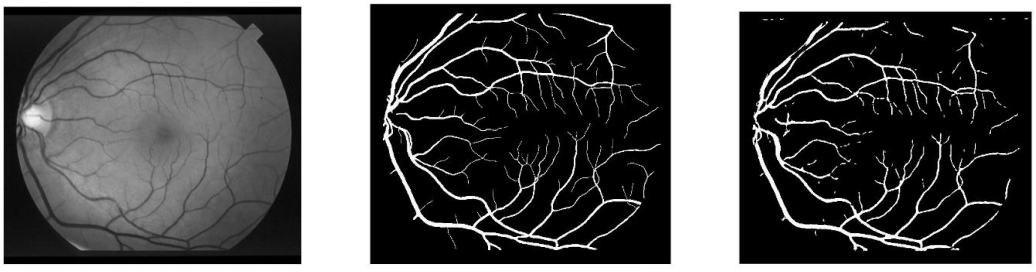

1(a) 1(b) 1(c)

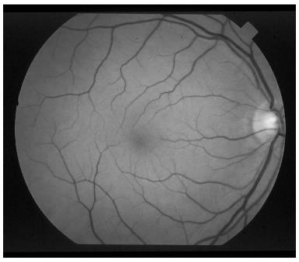

2(a)

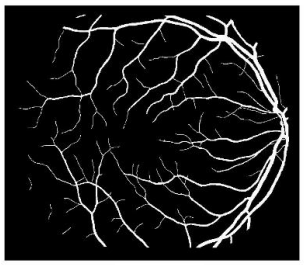

2(b)

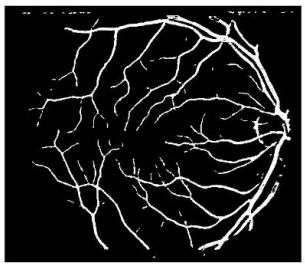

2(c)

Figure A.2: Figures 1 and 2 are STARE images 77 and 82, respectively. 1(a) and 2(a) are green channel images, 1(b) and 2(b) are ground truth images, 1(c) and 2(c) are results from supervised segmentation algorithm.

2. Unsupervised method

1(a)

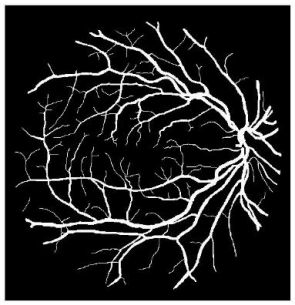

1(b)

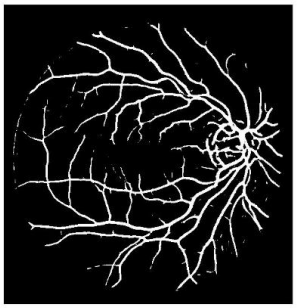

1(c)

2(a)

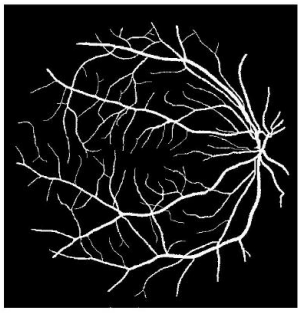

2(b)

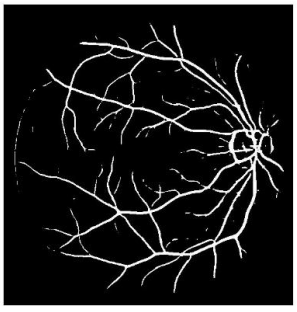

2(c)

Figure A.3: Figures 1 and 2 are DRIVE images 2 and 19, respectively. 1(a) and 2(a) are green channel images, 1(b) and 2(b) are ground truth images, 1(c) and 2(c) are results from unsupervised segmentation algorithm.

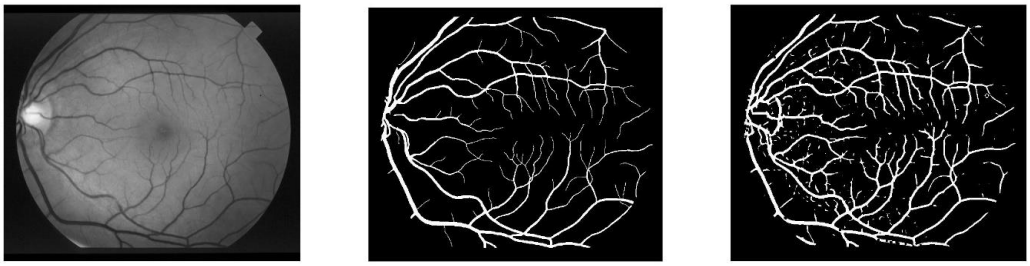

1(a) 1(b) 1(c)

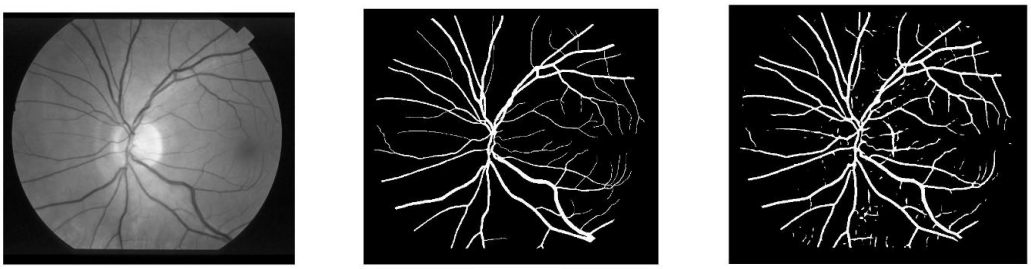

2(a) 2(b) 2(c)

Figure A.4: Figures 1 and 2 are STARE images 77 and 163, respectively. 1(a) and 2(a) are green channel images, 1(b) and 2(b) are ground truth images, 1(c) and 2(c) are results from unsupervised segmentation algorithm.

3. Matched filtering method

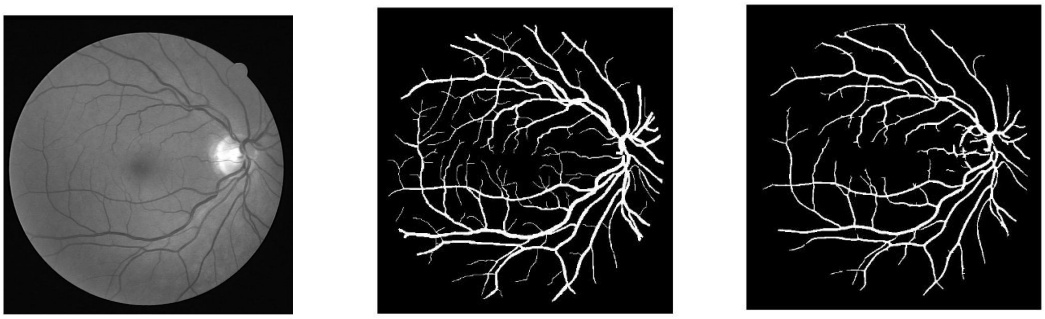

1(a) 1(b) 1(c)

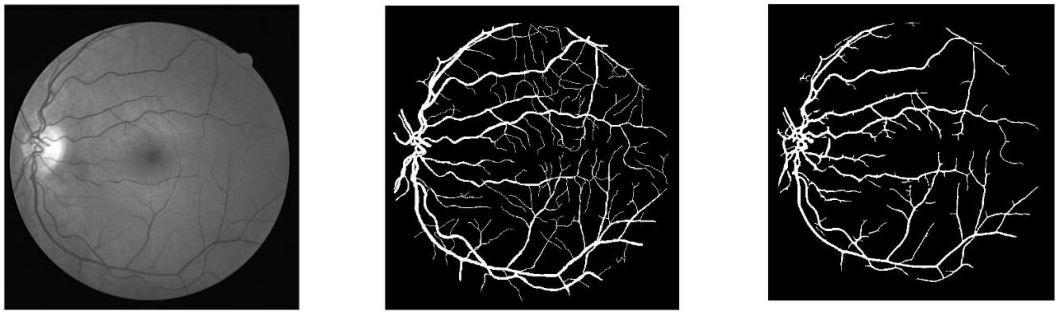

2(a) 2(b) 2(c)

Figure A.5: Figures 1 and 2 are DRIVE images 2 and 11, respectively. 1(a) and 2(a) are green channel images, 1(b) and 2(b) are ground truth images, 1(c) and 2(c) are results from matched filtering segmentation algorithm.

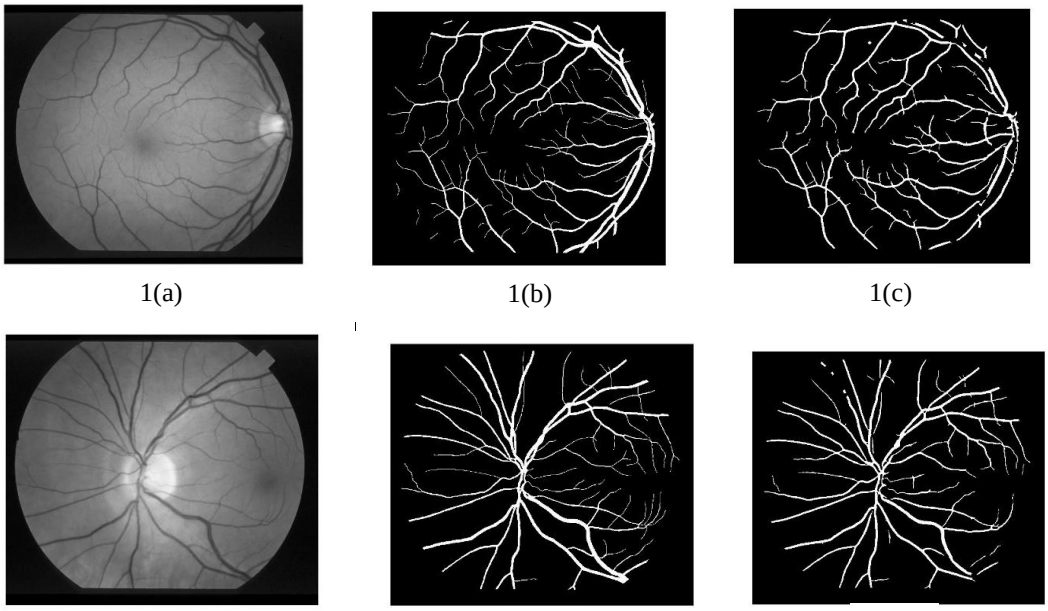

1(a) 1(b) 1(c)

2(a) 2(b) 2(c)

Figure A.6: Figures 1 and 2 are STARE images 82 and 163, respectively. 1(a) and 2(a) are green channel images, 1(b) and 2(b) are ground truth images, 1(c) and 2(c) are results from matched filtering segmentation algorithm.

Appendix B: Matlab codes for supervised method using gray-level and moment invariants with neural network

Filename: feature_generation.m

```
% Read image and generate mask
%-------------------------------------
image_file = '\Images\DRIVE\training\images\27_training.tif';
image = imread(image_file);
image = double(image)/255;

mask1 = image(:,:,1) > (50/255);
mask1 = imerode(mask1, strel('disk',3));

% Vessel Central Light Reflex Removal Start
%-----------------------------------------
green_channel_img = image(:,:,2);
struct_elem = strel('disk',3,8);
green_channel_img_open = dou-
ble(imopen(green_channel_img,struct_elem)); %Iy
%-----------------------------------------
% Vessel Central Light Reflex Removal End


%Background Homogenization start
%filtered using mean filter
%--------------------------
mean_filt = fspecial('average',[3 3]);
mean_filtered_img = filter2(mean_filt, green_channel_img_open);

%Define gaussian filter and perform convolution
%----------------------------------------------
gauss_filter = fspecial('gaussian', [9 9], 1.8);
conv_img = imfilter(mean_filtered_img, gauss_filter,'same');

%Applying mean filter of 69 x 69
%-------------------------------
mean_filt2 = fspecial('average',[69 69]);
mean_filtered_img2 = filter2(mean_filt2, conv_img);   % Ib
mean_filtered_img2 = mean_filtered_img2 .* mask1;

Isc = green_channel_img_open - mean_filtered_img2;    %Isc=Iy-Ib
Isc = Isc - min(Isc(:));
Isc = Isc / max(Isc(:));
mask_Isc = Isc .* mask1;

grayLevels = linspace(0,1,256);
max_Isc = grayLevels(hist(Isc(:)) == max(hist(Isc(:))));
Ih = Isc + .5 - max_Isc;
Ih(Ih<0) = 0;
Ih(Ih>1) = 1;
%---------------------------
%Background Homogenization end
```

```
%Vessel Enhancement start
%------------------------
comp_Ih = imcomplement((Ih));

se = strel('disk', 8);
top_hat_trans_comp_Ih = imtophat(comp_Ih, se);
Ive = top_hat_trans_comp_Ih;
%----------------------
%Vessel Enhancement end


% Gray Level Based Feature Extraction
%-----------------------------------
 [f1, f2, f3, f4, f5] = gray_level_features(Ih);

% Moment Invariants Based Feature Extraction
%-------------------------------------------
f6 = nlfilter(Ive, [17 17], @moment_feature_vec_f6);
f7 = nlfilter(Ive, [17 17], @moment_feature_vec_f7);

%Naming the matfiles as 'Drive_image_27_features.mat'
%---------------------------------------------
mat_file = 'Drive_image_27_features.mat';

%Saving the features into separate matfiles
%-------------------------------------------
save(mat_file,'f1', 'f2', 'f3', 'f4', 'f5', 'f6', 'f7', '-v6');
```

Filename: gray_level_features.m

```
% Gray-Level-Based Features calculation
function [f1, f2, f3, f4, f5] = gray_level_features(Ih)
% fi => Features

% f1(x,y) = Ih(x,y) - min{Ih(s,t)}
fun1 = @(x) min(x(:));
Ih_min = nlfilter( Ih, [9 9], fun1);
f1 = Ih - Ih_min;

% f2(x,y) = max{Ih(s,t)} - Ih(x,y)
fun2 = @(x) max(x(:));
Ih_max = nlfilter( Ih, [9 9], fun2);
f2 = Ih_max - Ih;

% f3(x,y) = Ih(x,y) - mean{Ih(s,t)}
fun3 = @(x) mean(x(:));
Ih_mean = nlfilter( Ih, [9 9], fun3);
f3 = Ih - Ih_mean;

% f4(x,y) = Standard deviation{Ih(s,t)}
fun4 = @(x) std(x(:));
Ih_std = nlfilter( Ih, [9 9], fun4);
f4 = Ih_std;

% f5(x,y) = Ih(x,y)
f5 = Ih;
```

Filename: moment feature vec f6.m

```
%First moment feature calculation
function f = moment_feature_vec_f6( I_ve)
%I_ve is vessel enhanced image
I_ve = double(I_ve);
gauss_matrix = fspecial('gaussian', [17 17], 1.7);
I_hu = I_ve .* gauss_matrix;
f = moment_features(I_hu, 6);
```

Filename: moment feature vec f7.m

```
%Second moment feature calculation
function f = moment_feature_vec_f7( I_ve)
I_ve = double(I_ve);
gauss_matrix = fspecial('gaussian', [17 17], 1.7);
I_hu = I_ve .* gauss_matrix;
f = moment_features(I_hu, 7);
```

Filename: moment features.m

```
%Moment features calculation
function f = moment_features(I_hu, count)
%I_hu is modified vessel enhanced image with a Gaussian filter
%count == 6 for sixth feature and count == 7 for seventh feature
if(count == 6)
    % First Moment
    n20 = normalized_central_moment(2, 0, I_hu);
    n02 = normalized_central_moment(0, 2, I_hu);
    phi_1 = n20 + n02;
    f = abs(log(phi_1));
elseif(count == 7)
    %Second Moment
    n20 = normalized_central_moment(2, 0, I_hu);
    n02 = normalized_central_moment(0, 2, I_hu);
    n11 = normalized_central_moment(1, 1, I_hu);
    phi_2 = (n20-n02)^2 + 4*(n11^2);
    f = abs(log(phi_2));
else
    error('Wrong input')
end
```

Filename: normalized central moment.m

```
function n_pq = normalized_central_moment( p, q, A)
%p = first order of moment
%q = second order of moment
%A = Modified vessel enhanced image (I_hu)

%if there is any 0's in image replace, it with very small number
%'eps'.
A(A == 0) = eps;

[m n] = size(A);
```

```
m00 = sum(sum(A));

%2-D Moment of order(p+q)
m10 = 0;              % m_pq where p=1 and q=0
m01 = 0;              % m_pq where p=0 and q=1
for a = 1:m
    for b = 1:n
        m10 = m10 + (a) * A(a,b);
        m01 = m01 + (b) * A(a,b);
    end
end

% Central moment
xx = m10/m00;
yy = m01/m00;

mu_00 = m00;
mu_pq = 0;
for ii = 1:m
    x = ii-xx;
    for jj = 1:n
        y = jj-yy;
        mu_pq = mu_pq + ((x)^p) * ((y)^q) * A(ii,jj);
    end
end

% Normalized cental moment of order(p+q)
gamma = (0.5*(p+q))+1;
temp = (mu_00^(gamma));
n_pq = mu_pq/temp;

%if n_pq equals 0, assign it very less value 'eps'
n_pq(n_pq == 0) = eps;
```

Filename: train data generate.m

```
% Train and test data are generated in same way using this function
% Generate train data for NN
load Drive_image_27_features.mat;

f1_mean = mean2(f1);
f2_mean = mean2(f2);
f3_mean = mean2(f3);
f4_mean = mean2(f4);
f5_mean = mean2(f5);
f6_mean = mean2(f6);
f7_mean = mean2(f7);

f1_std = std2(f1);
f2_std = std2(f2);
f3_std = std2(f3);
f4_std = std2(f4);
f5_std = std2(f5);
f6_std = std2(f6);
f7_std = std2(f7);

%Features normalized to zero mean and unit variance
```

```
new_f1 = (f1 - f1_mean)/f1_std;
new_f2 = (f2 - f2_mean)/f2_std;
new_f3 = (f3 - f3_mean)/f3_std;
new_f4 = (f4 - f4_mean)/f4_std;
new_f5 = (f5 - f5_mean)/f5_std;
new_f6 = (f6 - f6_mean)/f6_std;
new_f7 = (f7 - f7_mean)/f7_std;

train_data = [new_f1(:) new_f2(:) new_f3(:) new_f4(:) new_f5(:)
new_f6(:) new_f7(:)];
save('Drive_train_data_27.mat', 'train_data', '-v6');
```

Filename: target data generate.m

```
% Generates target data for training NN
manual = imread('\Images\DRIVE\training\1st_manual\27_manual1.gif');
manual_bw  = (manual == 255);
target_data = manual_bw(:);
save('Drive_target_data_27.mat', 'target_data', '-v6');
```

Filename: trainedNN.m

```
% Training the NN
% Loads train and target data
load Drive_train_data_27.mat;
load Drive_target_data_27.mat;

%Training and target data are transposed to allow NN to take data as
%a column vector
train_data = train_data';
target_data = target_data';

netN = feedforwardnet(15);
net = train(netN, train_data, target_data);
mat_file = 'Drive_27_trainedNN.mat';

%Saving the trained NN into separate matfiles.
save(mat_file, 'net', '-v6');
```

Filename: simulationNN.m

```
%Perform simulation over the test data using trained NN
%load test data and trained NN
load Drive_test_data_02.mat;
load Drive_27_trainedNN.mat;

%read ground truth data
img = imread('\Images\DRIVE\test\1st_manual\02_manual1.gif');
[row col] = size(img);

test_data = test_data';

% Simulation
Y = net(test_data);
```

```
% For DRIVE
threshold = (Y > 0.53);
% For STARE
%threshold = (Y > 0.43);
threshold = double(threshold);
reshape_threshold_img = reshape(threshold, row, col);

final_segmented_image = post_processing(reshape_threshold_img);
figure, imshow(final_segmented_image);

final_segmented_image = double(final_segmented_image);
[Se, Sp, ppv, Npv, Acc] = performance_measure(final_segmented_image,
img)
```

Filename: post processing.m

```
% Post Processing step
function x = post_processing(I)
%I = segmented image
%Iterative filling; at least neighbor 6 pixels must be vessel to
%consider a center pixel as a vessel
fill = nlfilter(I, [6 6], @iterative_fill);

%artifact removal: Each connected region to an area below 10 is
%reclassified as non-vessels
final_vessel_segmented_image = bwareaopen(fill, 10);
x = final_vessel_segmented_image;
```

Filename: performance measure.m

```
function [Se, Sp, Ppv, Npv, Acc] = performance_measure(final_image,
target_image)
% Se = Sensitivity
% Sp = Specificity
% Ppv = Positive predictive value
% Npv = Negative predictive value
% Acc = Accuracy
% final_image = post processed final image
% target_image = gold standard image

TP = 0;     %True Positive
FP = 0;     %False Positive
FN = 0;     %False Negative
TN = 0;     %True Negative

[row col] = size(target_image);
target_image = im2bw(target_image);
for x = 1:row
    for y = 1:col
        if((final_image(x,y)== 1) && (target_image(x,y) == 1))
            TP = TP + 1;
        else if((final_image(x,y)== 1) && (target_image(x,y) == 0))
                FP = FP + 1;
            else if((final_image(x,y)==0)&&(target_image(x,y) ==1))
```

```
                    FN = FN + 1;
                else
                    TN = TN + 1;
                end
            end
        end
    end
end

Se = TP /(TP + FN);
Sp = TN /(TN + FP);
Ppv = TP /(TP + FP);
Npv = TN /(TN + FN);
Acc = (TP + TN)/(TP + FN + TN + FP);
```

Appendix C: Matlab codes for unsupervised method using local entropy and gray-level co-occurrence matrix

Filename: Main_unsupervised_method.m

```
% Main method
img = imread('\Images\DRIVE\test\images\01_test.tif');
img = img(:,:,2);
img = double(img)/255;

mask = img > (20/255);  % For Drive
%mask = img > (35/255);  % For stare
mask = double(imerode(mask, strel('disk',3)));

% Matched filtering
extractedVessel = MatchFiltered(img, 1.2, 9, 12);

% Element-wise multiplication
newExtractedVessel = extractedVessel.*mask;

% Normalization
normVessel = newExtractedVessel - min(newExtractedVessel(:));
normVessel = normVessel / max(normVessel(:));
normVessel = round(normVessel * 255);

grayValue = (unique(normVessel(:)))';
grayValueCount = numel(grayValue);

c = grayValueCount;

t = graycomatrix(newExtractedVessel, 'GrayLimits',
[min(newExtractedVessel(:)) max(newExtractedVessel(:))], 'Num-
Levels', c);

% Adding entire values of the co-occurence matrix
t_sum = sum(t(:));

% Normalizing the co-occurrence matrix
P = zeros(c,c);
for i = 1:c
    for j = 1:c
        P(i,j) = t(i,j)/t_sum;
    end
end

t_JRE = generate_Tjre(P, c);

% Thresholding
final_segmented_img = newExtractedVessel > t_JRE;

g_truth = imread('\Images\DRIVE\test\1st_manual\01_manual1.gif');

% performance_measure function is same as used in supervised method
[Se, Sp, Ppv, Npv, Acc] = performance_measure(final_segmented_img,
g_truth);
```

Filename: matched filtered.m

```
function[vess] = match_filtered(img,sigma,yLengthForMF, numOfDirec-
tions)
%    Retinal vessel extraction by matched filter
%
%       Inputs:
%          img                -   input imgage
%          sigma              -   scale value
%          yLengthForMF       -   length of neighborhood along y-
%                                  axis of MF
%          numOfDirections    -   number of orientations
%
%      Output:
%          vess               -   vessels extracted

if isa(img, 'double')~=1
    img = double(img);
end

[rows, cols] = size(img);

MatchFilterRes(rows, cols, numOfDirections) = 0;
for i = 0:numOfDirections-1
    matchFilterKernel = match_filter_kernel_generate(sigma, yLength-
      ForMF, pi/numOfDirections*i);
    MatchFilterRes(:,:,i+1) = conv2(img, matchFilterKernel, 'same');
end

[maxMatchFilterRes] = max(MatchFilterRes, [], 3);
vess = maxMatchFilterRes;
```

Filename: match filter kernel generate.m

```
function[kernel]=match_filter_kernel_generate(sigma, YLength, theta)
%    MF kernel construction
%
%        Inputs:
%            sigma   - scale value
%            YLength - length of neighborhood along y-axis
%            theta   - orientation
%
%        Output:
%            kernel  - MF kernel
%
%    YLength should be an odd integer

widthOfTheKernel = ceil(sqrt( (6*ceil(sigma)+1)^2 + YLength^2));
if mod(widthOfTheKernel,2) == 0
    widthOfTheKernel = widthOfTheKernel + 1;
end
halfLength = (widthOfTheKernel - 1) / 2;
row = 1;
for y = halfLength:-1:-halfLength
    col = 1;
```

```
    for x = -halfLength:halfLength
        xPrime = x * cos(theta) + y * sin(theta);
        yPrime = y * cos(theta) - x * sin(theta);
        if abs(xPrime) > 3.5*ceil(sigma)
            matchFilterKernel(row,col) = 0;
        elseif abs(yPrime) > (YLength-1) / 2
            matchFilterKernel(row,col) = 0;
        else
            matchFilterKernel(row,col) = -exp(-.5*(xPrime/sigma)^2)
            / (sqrt(2*pi)*sigma);
        end
        col = col + 1;
    end
    row = row + 1;
end
mean = sum(sum(matchFilterKernel))/sum(sum(matchFilterKernel < 0));
for i = 1:widthOfTheKernel
    for j =1:widthOfTheKernel
        if matchFilterKernel(i,j) < 0
            matchFilterKernel(i,j) = matchFilterKernel(i,j) - mean;
        end
    end
end
kernel = matchFilterKernel;
```

Filename: generate Tjre.m

```
function T = new_generate_Tjre( P, L)
%% Probabilities associated with each quadrants
x = 1;
T_JRE = zeros(L);
for th = 1:L
    PtB = sum(sum(P(1:th, th+1:L)));
    PtD = sum(sum(P(th+1:L, 1:th)));

    qtB = PtB / ((th+1)*(L-th-1));
    qtD = PtD / ((L-th-1)*(L+1));

    temp = -( PtB*log(qtB) + PtD*log(qtD))/10;
    if temp > 0
        T_JRE(x) = temp;
        x = x + 1;
    end
end

T = max(T_JRE(:));
end
```

Appendix D: Matlab codes for matched filtering method using first order derivative of Gaussian

Filename: Main_matched_filtering_method.m

```
img = imread('\Stare\StareImages\im0162.ppm\im0162.ppm');
img = img(:,:,2);

% Mask for the fundus image generation
level = graythresh(img) - 0.06;
mask = im2bw(img,level);
gTruth = imread('\Stare\labels-ah\im0162.ah.ppm\im0162.ah.ppm');
se = strel('disk',4);
mask=imerode(mask,se);

%MatchFilterWithGaussDerivative(image, sigma, yLength, numOfDirec-
tions, mask, c_value, threshold value_for_regionprop)
thick_vess  = MatchFilterWithGaussDerivative(img, 1.5, 9, 12, mask,
               2.3, 30);
figure, imshow(thick_vess)
thin_vess = MatchFilterWithGaussDerivative(img, 1, 4, 12, mask, 2.3,
            30);
figure, imshow(thin_vess)

vess = thick_vess | thin_vess;
figure, imshow(vess)

[tpr tnr acc] = performance_measure(vess, mask, gTruth)
```

Filename: MatchFilterWithGaussDerivative.m

```
function [vess] = MatchFilterWithGaussDerivative(img, sigma,
yLength, numOfDirections, mask, c_value, t)

%  Retinal vessel extraction by matched filter with first-order
%  derivative of Gaussian
%
%       Inputs:
%          img                -   input imgage
%          sigma              -   scale value
%          yLength            -   length of neighborhood along y-
%                                  axis
%          numOfDirections    -   number of orientations
%          mask               -   image mask
%          c_value            -   c value
%          t                  -   threshold value of region props
%
%      Output:
%          vess               -   vessels extracted


if isa(img,'double')~=1
    img = double(img);
end
```

```
[rows,cols] = size(img);

MatchFilterRes(rows,cols,numOfDirections) = 0;
GaussDerivativeRes(rows,cols,numOfDirections) = 0;

for i = 0:numOfDirections-1
      matchFilterKernel = MatchFilterAndGaussDerKernel(sigma,
      yLength, pi/numOfDirections*i, 0);
      gaussDerivativeFilterKernel = MatchFilterAndGaussDerKer-
      nel(sigma, yLength, pi/numOfDirections*i, 1);
      MatchFilterRes(:,:,i+1) = conv2(img,matchFilterKernel,'same');
      GaussDerivativeRes(:,:,i+1) =
      (conv2(img,gaussDerivativeFilterKernel,'same'));
end

maxMatchFilterRes = max(MatchFilterRes,[],3);
maxGaussDerivativeRes = max(GaussDerivativeRes,[],3);

D = maxGaussDerivativeRes;

W = fspecial('average', 31);
Dm = imfilter(D, W);

%Normailzation
Dm = Dm - min(Dm(:));
Dm = Dm/max(Dm(:));

%muH = mean value of response image H
H = maxMatchFilterRes;
c = c_value;
muH = mean(H(:));

Tc = c * muH;
T = (1 + Dm) * Tc;

Mh = (H >= T);

vess = Mh & mask;

se = strel('square',3);
vess = imclose(vess,se);
vess = bwmorph(vess,'close');
[L num] = bwlabel(vess, 8);
prop = regionprops(L, 'Area');
idx = find([prop.Area] > t);
vess = ismember(L,idx);
```

Filename: MatchFilterAndGaussDerKernel.m

```
function [kernel] = MatchFilterAndGaussDerKernel(sigma, YLength,
theta, type)
%
%    MF and FDOG kernel construction
%
%        Inputs:
%             sigma      -   scale value
%             YLength    -   length of neighborhood along y-axis
```

```
%             theta      -   orientation
%             type       -   MF or FDOG
%
%        Output:
%             kernel     -   Gaussian kernel

if type == 0
    widthOfTheKernel = ceil(sqrt((6*ceil(sigma)+1)^2 + YLength^2));
    if mod(widthOfTheKernel,2) == 0
        widthOfTheKernel = widthOfTheKernel + 1;
    end
    halfLength = (widthOfTheKernel - 1) / 2;
    row = 1;
    for y = halfLength:-1:-halfLength
        col = 1;
        for x = -halfLength:halfLength
            xPrime = x * cos(theta) + y * sin(theta);
            yPrime = y * cos(theta) - x * sin(theta);
            if abs(xPrime) > 3.5*ceil(sigma)
                matchFilterKernel(row,col) = 0;
            elseif abs(yPrime) > (YLength-1) / 2
                matchFilterKernel(row,col) = 0;
            else
                matchFilterKernel(row,col) = -exp(-
                .5*(xPrime/sigma)^2)/(sqrt(2*pi)*sigma);
            end
            col = col + 1;
        end
        row = row + 1;
    end
    mean=sum(sum(matchFilterKernel))/sum(sum(matchFilterKernel<0));
    for i = 1:widthOfTheKernel
        for j =1:widthOfTheKernel
            if matchFilterKernel(i,j) < 0
                matchFilterKernel(i,j)=matchFilterKernel(i,j)- mean;
            end
        end
    end
    kernel = matchFilterKernel;
else
    widthOfTheKernel = ceil(sqrt( (6*ceil(sigma)+1)^2 + YLength^2));
    if mod(widthOfTheKernel,2) == 0
        widthOfTheKernel = widthOfTheKernel + 1;
    end
    halfLength = (widthOfTheKernel - 1) / 2;
    row = 1;
    for y = halfLength:-1:-halfLength
        col = 1;
        for x = -halfLength:halfLength
            xPrime = x * cos(theta) + y * sin(theta);
            yPrime = y * cos(theta) - x * sin(theta);
            if abs(xPrime) > 3.5*ceil(sigma)
                GaussDerivativeKernel(row,col)  = 0;
            elseif abs(yPrime) > (YLength-1) / 2
                GaussDerivativeKernel(row,col)  = 0;
            else
```

```
                GaussDerivativeKernel(row,col)= -exp(-
                   .5*(xPrime/sigma)^2)*xPrime/(sqrt(2*pi)*sigma^3);
            end
            col = col + 1;
        end
        row = row + 1;
    end
    kernel = GaussDerivativeKernel;
end
```

Filename: performance.m

```
function [tpr fpr accu] = performance(img, mask, gTruth)
%
%    Performance measurement
%
%         Inputs:
%             img      -   input image
%             mask     -   image mask
%             gTruth   -   ground truth
%
%         Outputs:
%             tpr      -   true positive rate
%             fpr      -   false positive rate
%             accu     -   accuracy

img = logical(img);
mask = logical(mask);
gTruth = logical(gTruth);
[index] = find(mask(:) == 1);
tpr = sum(gTruth(img(:) == 1)) / sum(gTruth(index) == 1);
accu = sum(img(index) == gTruth(index)) / length(index);
fpr = sum(gTruth(img(:) == 1 & mask(:) == 1) == 0) /
      sum(gTruth(index) == 0);
```